Ricerca di Sistema elettrico

TAPIRO: feasibility study of minor actinides irradiation campaign

M. Carta, P. Console Camprini, V. Fabrizio,
O. Florani, A. Grossi, V. Peluso, A. Santagata,
A. Boccia, A. Gardini,
C. Bethaz, P. Ravetto

TAPIRO: FEASIBILITY STUDY OF MINOR ACTINIDES IRRADIATION CAMPAIGN

M. CARTA, P. CONSOLE CAMPRINI, V. FABRIZIO, O. FIORANI, A. GROSSI, V. PELUSO, A. SANTAGATA - ENEA,

F. BOCCIA, A. GANDINI - UNIVERSITA' DI ROMA LA SAPIENZA, C. BETHAZ, P. RAVETTO - POLITECNICO DI TORINO

Settembre 2015

TAPIRO: feasibility study of minor actinides irradiation campaign.

Tipologia del documento: Technical Note / Rapporto Tecnico
Collocazione contrattuale: Accordo di Programma ENEA-MISE su sicurezza nucleare e reattori di IV generazione.
Argomenti trattati: Reattori di ricerca, Neutronica, Generation IV

Sommario

All'interno di un gruppo di esperti della NEA, sulla gestione degli Attinidi Minori, è stata avviata una collaborazione tra ENEA e CEA per lo studio di fattibilità di una campagna di irraggiamenti presso il reattore di ricerca RSV-TAPIRO presente nel C:R. Casaccia dell'ENEA. Questo studio è stato suddiviso in due parti, la prima parte ha riguardato la caratterizzazione neutronica del reattore TAPIRO attraverso l'utilizzo di diversi codici di calcolo (ERANOS deterministico, Serpent e MCNP monte carlo) applicando entrambe le metodologie di calcolo deterministica e stocastica; la seconda parte ha riguardato la schematizzazione di alcuni campioni di attinidi minori, caricati con diversi isotopi, forniti dal CEA, e precedentemente utilizzati per la campagna sperimentale francese OSMOSE, così da valutare l'entità delle diverse sezioni d'urto e della loro attivazione.

Summary

In the framework of the NEA Expert Group on Integral Experiments for Minor Actinide Management (EGIEMAM) a joint collaboration between ENEA (Italian National Agency for New Technologies, Energy and Sustainable Economic Development) and CEA (French Alternative Energies and Atomic Energy Commission) was established to study the feasibility of a MAs irradiation campaign in the TAPIRO fast neutron source research reactor located at the ENEA Casaccia centre. This report provides the neutronic characterization of the TAPIRO reactor by two different codes (ERANOS and Serpent) and modelling the irradiation, in different TAPIRO irradiation channels, of some CEA samples coming from the French experimental campaign OSMOSE, loaded with different contents of MAs, in order to know their capture cross section.

Note

Autori:

M. Carta, P. Console Camprini, V. Fabrizio, O. Fiorani, A. Grossi, V. Peluso, A. Santagata (ENEA)

F. Boccia, A. Gandini (Università di Roma 'La Sapienza')

C. Bethaz, P. Ravetto (Politecnico di Torino)

Copia n.			In carico a:			
2			NOME			
			FIRMA			
1			NOME			
			FIRMA			
0	EMISSIONE	21-09-2015	NOME	M. Carta	M. Tarantino	M. Tarantino
			FIRMA			
REV.	DESCRIZIONE	DATA		REDAZIONE	CONVALIDA	APPROVAZIONE

Index

1. Introduction.

The reduction of the nuclear waste is one of the most important nuclear issues, followed by the current worldwide R&D for the closed fuel cycle fulfillment and the IV Generation reactors development. The spent fuel discharged from nuclear power plants constitutes the main contribution to nuclear waste. The high radiotoxicity of the spent fuel is due to plutonium and some minor actinides (MAs) such as neptunium, americium and curium, above all. One way to reduce their hazard is to transmute MAs in appropriate nuclear reactors. To allow the MAs transmutation an important effort have been done on the nuclear data due to the poor knowledge in this field. Several NEA and IAEA Working Groups addressed these issues, even recommending integral measurements, complementary to parallel efforts for differential measurements, for the several nuclides of MAs from viewpoints of design of transmutation systems and of fuel cycles. In the framework of one of the NEA Expert Group on Integral Experiments for Minor Actinide Management (EGIEMAM) the feasibility of MAs irradiation campaign in TAPIRO research reactor is carried out in this report.
This work is divided into two different parts, the first one consider the neutronic analysis by two different code, the deterministic ERANOS and the Monte Carlo SERPENT codes; the second one carried out by FISPACT code allows to evaluate the activation of different MAs samples, supplied by CEA.

2. TAPIRO research reactor.

TAPIRO (**TA**ratura**PI**la**R**apida a potenzazer**O)**, a fast nuclear research reactor located at C.R ENEA-CASACCIA, was developed by ENEA, based on the project of the Argonne Fast Source Reactor (AFSR, Idaho falls). Thestartup was in 1971 and is currently used in supporting experimental programs finalized to [1]:

- validation of calculation codes for studies on the development of Gen-IV reactors (ADS systems);
- analysis on fast neutrons damages on materials and electronics components;
- training and experiences for nuclear engineering courses.

In the following picture a view of TAPIRO reactor room is showed in Figure 1:

Figure 1 - TAPIRO reactor room.

It has a maximum power of 5 kW with a neutron flux of 4 x 10^{12} n/(cm^2 s) in the centre of the core. The core is cylindrical with a diameter of about 12 cm and a similar height. It is made with metallic uranium (98.5 % uranium and 1.5 % molybdenum) with an enrichment of 93.5 % in ^{235}U. It consists of 2 parts: the upper part is fixed while the lower one is movable. The core is surrounded by a double layer of copper reflector and by an external biological shield of borate concrete. It is refrigerated by helium. The reactor is equipped with 2 shim rods, 2 safety rods and a regulating rod. These rods are realized with the same material of the reflector and the reactor is controlled increasing or reducing the leaks of neutrons.

A horizontal section of the reactor at 1 m from the floor is showed in Figure 2:
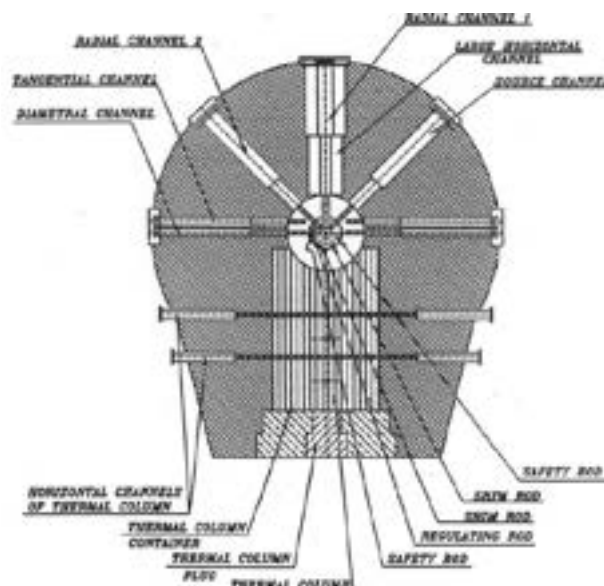

Figure 2 - Horizontal Section of TAPIRO parallel to the floor.

To allow irradiation experiences, the system has different channels, located in different positions; they are realized with a metallic cylindrical clad and they are filled with plugs made of copper, in the

reflector's area, and of shielding material in the external part. The copper part of each plug is removable to permit the insertion of sample material or detectors used for experiences. An important characteristic of the channels is that their sections are gradually reduced to cut down the gamma ray streaming effect. The main channels are shown in Table1) [1]:

Name	Position	Penetration
Diametral channel (D.C.)	Piercing. Horizontal. Diametral in the core.	Inner and outer fixed reflector. Core.
Tangential channel	Piercing. Horizontal. 50 mm above core mid-plane. Parallel to D.C. 106 mm from core axis.	Inner and outer fixed reflector.
Radial channel 1 (R.C.1)	Radial. Horizontal on core mid-plane, at 90° with respect to D.C.	Inner and outer fixed reflector, up to 93 mm from core axis.
Radial channel 2	Radial. Horizontal on core mid-plane, at 50° with respect to R.C.1.	Outer fixed reflector,up to 228 mm from core axis.
Grand Horizontal Channel (G.H.C.)	Radial. Concentric with R.C.1.	Up to reflector outer surface
Grand Vertical Channel (G.V.C.)	Above core, on the same axis.	Outer fixed reflector, up to 100 mm from upper core base.
Thermal column	Horizontal.	Shield, up to outer reflector
Irradiation cavity	On safety plug upper base.	7.4 mm

Table 1 - TAPIRO experimental channels

3. The ERANOS code.

The European Reactor Analysis Optimized calculation System, ERANOS [3], has been developed and validated with the aim of providing an appropriate basis for neutronic calculations of current fast (and thermal) reactor cores. It consists of data libraries, deterministic codes and calculation procedures developed within a European framework and it meets the needs expressed by the industrialists and the teams working on the design of fast reactors, present and future.
ERANOS is written using the ALOS software which requires only standard FORTRAN compilers and include advanced programming features. It allows, with the use of LU user's language, to perform programs of R&D in reactor physics without needing specific development.

3.1 Architecture.

Fast reactor core, shielding and fuel cycle calculations can be performed with the ERANOS system. A modular structure was adopted for easier evolution and incorporation of new functionalities.
Blocks of data can be created (data SETs) or used by different modules or by the user with LU control language. Programming and dynamic memory allocation are performed with the use of the ESOPE language. It can be possible to make an external temporary storage or permanent storage with the

GEMAT and ARCHIVE functions, respectively. ESOPE, LU, GEMAT, and ARCHIVE are all part of the ALOS software.

This type of structure, based on a modular system, allows to link together different modules in procedures corresponding to recommended calculation routes ranging from fast-running and moderately-accurate 'routine' procedures to slow-running but highly-accurate 'reference' procedure.

The main contents of ERANOS-2.2 package are:

- nuclear data libraries, multi group cross sections from ERALIB1, ENDF-/B-VI.8, JEF-2.2, JEF-3.1 evaluated nuclear data files, and other specific data;
- a cell and lattice code ECCO;
- reactor flux solvers (diffusion, S_n transport, nodal variational transport);
- a burn-up module;
- different processing modules (material and neutron balance, breeding gains,…);
- perturbation theory and sensitivity analysis modules;
- core follow-up modules;
- a fine burn-up analysis subset named MECCYCO (mass balances, activities, decay heat, dose rate).

Each nuclear data package contains four neutron cross section libraries obtained by processing the corresponding nuclear data files by the NJOY and CALENDF codes and they are:

- a 1968 energy group library containing 41 main nuclides;
- a 33 energy group library containing 246 nuclides, including pseudo fission products;
- a 175 energy group library used for shielding calculation only;
- a 172 energy group library used mainly for thermal spectrum calculations.

3.2 Cell Calculations.

ERANOS code has been developed within the European Collaboration on Fast Reactors over the past 30 years or so. It consists of data libraries, deterministic codes and calculation procedures.

ERANOS is a deterministic code system, neutron physics calculations are performed at the cell/lattice level and at the core level. The development of the ECCO Code was decided in 1985 by several R&D teams working within the framework of the European Fast Reactor Collaboration [3].

ECCO [4], European Cell COde, is the cell code allowing to calculate the cross sections matrices to be used in spatial core calculations performed by different ERANOS modules.

First of all, it is necessary to provide to ECCO media composition (homogeneous mixtures), expansion coefficients and geometric description of the cell. Then the cross sections are calculated by using the defined media and the associated nuclear data libraries by means of the collision probability method.

The nuclear data libraries are available at different temperature (293.6, 573.6, 973.6, 1473.6, 2973.6 K) to take into account the Doppler effect for the main nuclides.

An ECCO calculation corresponds to a succession of STEPs, and for each STEP one can select energy structure, cell geometry (heterogeneous or homogeneous), flux calculation type, and so on.

Many type of geometry are available within the ECCO code:

- 1D, plane or cylindrical calculated by exact collision probabilities method;
- 2D, rectangular lattice made of cylindrical and/or square pins within a square tube, hexagonal lattice made of cylindrical pins within a hexagonal sheet calculated by approximate collision probability method (Roth and double step methods);
- 3D, XYZ and HEX-Z calculated by approximate collision probability method.

The user has the possibility to chain several calculation steps so as to produce design or reference calculations, or even to use specific capabilities, according to the need of the study.
A route is a recommended way to perform ECCO calculations. The first route is the "reference" one that does not care about the time calculation and treats the heterogeneous cell at fine energy group level (1968 groups). The second route is the "project" or "design" one in which some simplifying hypotheses are assumed, the elastic slowing down is treated in a homogeneous geometry but at fine group level, the self-shielding is treated in a heterogeneous geometry at broad group level (33 groups).

3.3 Static Calculations.

ERANOS allows several types of flux calculations: diffusion and transport calculations with different methods; in each case can be addressed external source, up-scattering and adjoint calculations. For all geometries, 1D plane, cylindrical and spherical, 2D RZ, R-theta, rectangular lattice XY, hexagonal lattice, and 3D rectangular lattice XYZ, hexagonal-Z can be used finite difference diffusion solvers. In 1D and in some 2D geometries, like RZ and XY, finite difference S_n transport calculations can be performed by means of the BISTRO [5] code. The physics of thermal and fast reactors require the capability to solve the transport equation in accurate manner for different 2D and 3D geometries; variational nodal methods are well adapted for these topics because of the reduced numbers of unknowns used and the good accuracy in the solution by using high order approximation for spatial and angular expansions of flux and current in the node.
Both 2D (XY and hexagonal) and 3D (XYZ and hexagonal-Z) geometries are available within the TGV/VARIANT variational nodal module. The module performs direct flux calculations, with and without an external source, and adjoint calculations, and is possible to set up several parameters for different types of analyses. The computing time, in comparison with other methods devoted to the transport equation solution (like S_n), is very competitive.

4. The Serpent code.

Serpent is a three-dimensional continuous-energy Monte Carlo reactor physics burnup calculation code, developed at VTT Technical Research Centre of Finland since 2004. [6]
The suggested applications of Serpent include:

- Spatial homogenization and group constant generation for deterministic reactor simulator calculations
- Fuel cycle studies involving detailed assembly-level burnup calculations
- Validation of deterministic lattice transport codes
- Full-core modeling of research reactors, SMR's, and other closely coupled systems

- Coupled multi-physics applications (available in Serpent 2)
- Educational purposes and demonstration of reactor physics phenomena.

Similar to other Monte Carlo codes, such as MCNP and Keno-VI, Serpent uses a universe-based combinatorial solid geometry (CSG) model, which allows the description of practically any two- or three-dimensional fuel or reactor configuration. The geometry consists of material cells, defined by elementary quadratic and derived macrobody surface types.

The code also provides some additional geometry features specifically for fuel design. These features include simplified definition of cylindrical fuel pins and spherical fuel particles, square and hexagonal lattices for LWR and fast reactor geometries, and circular cluster arrays for CANDU fuels.

The random dispersion of microscopic fuel particles in high-temperature gas cooled reactor fuels and pebble distributions in pebble-bed type HTGR cores can be modeled using geometry types specifically designed for the task.

4.1 History of the Serpent project

The development of Serpent started at VTT in 2004, under the working title "Probabilistic Scattering Game". The name was later changed to Serpent, due to the various ambiguities related to the PSG acronym.

The main reason to start developing a new Monte Carlo neutron transport code from scratch was the fact that the general-purpose codes available at that time were not particularly well suited for lattice physics applications. Group constant generation requires the combination of several user-definedreaction rate tallies and the estimation of combined statistical errors becomes complicated. The overall calculation time increases dramatically along with the number of tally definitions, and the calculation of certain parameters, such as scattering matrices, diffusion coefficients and effective delayed neutron fractions lies completely beyond the standard tally capabilities.

The source code was completely re-written by the end of 2005. The new version included a bound-atom scattering model for moderator isotopes. Parallel calculation using the Message Passing Interface (MPI) was also implemented.

Another major improvement was a new geometry routine that could overcome the localized absorber problems of delta-tracking in simple lattice geometries.

The current version of Serpent 1 began to formulate when the source code was completely re-written for a second time by the beginning of 2008. A persistent methodological flaw in the free-gas scattering model was corrected, which finally reduced the differences to MCNP results to the level of statistical accuracy. The old geometry routine was also replaced by a more general approach based on the combination of delta-tracking and the conventional surface tracking method.

The development ofburnup calculation routines began in early 2008. The first version was based on an external coupling to the ORIGEN2 depletion code. It was soon decided, however, that the code should also have the capability to run burnup calculation as a complete stand-alone application.

A pre-release version (1.0.0) of the Serpent code was made available to some universities and research institutes in October 2008. The code was submitted for public distribution to the NEA Data Bank in April 2009 and released one month later [6].

4.2 Monte Carlo method in Serpent

The Monte Carlo simulation can be run in k-eigenvalue criticality source or external source mode. Neutron transport is based on a combination of conventional surface-to-surface ray-tracing and the Woodcock delta-tracking method. The tracking routine has proven efficient and well suited for geometries where the neutron mean-free-path is long compared to the dimensions.

The main drawback of delta-tracking is that the track-length estimate of neutron flux is not available and reaction rates have to be calculated using the potentially less-efficient collision estimator. This is usually not a problem in reactor calculations when reaction rates are scored in regions of high collision density. However, the efficiency of the collision estimator becomes poor in small or optically thin volumes located far or isolated from the active source.

The continuous-energy Monte Carlo method has been used for criticality safety analyses, radiation shielding and dose rate calculations, detector modeling and the validation of deterministic transport codes for decades.

The main motivator is usually the need to model geometry and interaction physics to within maximum accuracy, often regardless of the computational cost. Monte Carlo codes are well suited for the job, with the capability to handle complicated three-dimensional geometries and to model neutron interactions at the microscopic level without major approximations. In fact, Monte Carlo codes are often used to complement or even replace experimental measurements.

The computational requirements for reactor analysis, in particular the modeling of operating power reactors, are considerably higher. The strong coupling between neutronic, thermal hydraulics and fuel behavior means that the transport problem cannot be solved separately, and even though considerable efforts are devoted to developing various multi-physics calculation systems, the Monte Carlo method cannot yet be considered a practical option for routine design and safety analyses of large LWR cores. The traditional approach to reactor analysis relies instead on a multi-stage calculation scheme, where the complexity of transport physics is gradually simplified, while simultaneously increasing the scale of the modeled system. In practice, the calculation sequence is divided into:

1. Spatial homogenization, where the interaction physics at the fuel assembly level is condensed into a set of assembly-specific multi-group constants;

2. Core simulation, where the full-scale neutronic solution obtained using diffusion theory or other simplified transport method is iteratively coupled to thermal hydraulics.

The same code and cross section data can be used for modeling any fuel or reactor configuration without compromising the reliability of the calculation scheme. The particle transport simulation in is inherently three-dimensional, which makes it possible to capture the effects of axial heterogeneities. [7]

4.3 Interaction physics

Serpent reads continuous-energy cross sections from ACE format data libraries, based on JEF-2.2, JEFF-3.1, JEFF-3.1.1, ENDF-VI.8 and ENDFBVII.

The interaction physics is based on classical collision kinematics, ENDF reaction laws and probability table sampling in the unresolved resonance region.

Interaction data is available for 432 nuclides at 6 temperatures between 300 and 1800K. Thermal bound-atom scattering data is included for light and heavy water and graphite.

Continuous-energy cross sections in the library files are reconstructed on a unionized energy grid, used for all reaction modes. The use of a single energy grid results in a major speed-up in calculation, as the number of CPU time consuming grid search iterations is reduced to minimum. Macroscopic cross sections for each material are pre-generated before the transport simulation.

Instead of calculating the cross sections by summing over the constituent nuclides during tracking, the values are read from pre-generated tables, which is another effective way of improving the performance.

A built-in Doppler-broadening preprocessor routine allows the conversion of ACE format cross sections into a higher temperature. This capability results in a more accurate description of the interaction physics in temperature sensitive applications, as the data in the cross section libraries is available only in 300K intervals.

5. MCNP code

MCNP6.1[8] is a general-purpose Monte Carlo N-Particle which is a worldwide reference for radiation transport simulations and nuclear components design and modelling. In fact, this code is used for neutron, photon, electron, or coupled neutron/photon/electron transport. Thus, the code deals with transport of neutrons, gamma rays, and coupled transport, i.e., transport of secondary gamma rays resulting from neutron interactions. The MCNP code can also treat the transport of electrons, both primary source electrons and secondary electrons created in gamma-ray interactions.

The code treats an arbitrary three-dimensional configuration of materials in geometric cells bounded by first- and second-degree surfaces and fourth-degree elliptical tori.

MCNP simulation – as well as a standard Monte Carlo one – is constructed starting from following aspects:
- geometry definition
- materials description and cross-section selection (nuclear data)
- location and characteristics of the neutron, photon, electron source
- type of answers or tallies to be obtained through the simulation
- variance reduction techniques implemented to improve calculation efficiency

System geometry is constructed by the user through cells defined by the intersections, unions, and complements of the regions bounded by the surfaces. Surfaces are defined by supplying coefficients to the analytic surface equations or, for certain types of surfaces, known points on the surfaces. MCNP also provides a macro-body capability, where basic shapes such as spheres, boxes, cylinders, etc., may be combined using boolean operators.

Pointwise cross-section data typically are used, although group-wise data also are available. For neutrons, all reactions given in a particular cross-section evaluation are accounted for. Thermal neutrons are described by both the free gas and $S(\alpha,\beta)$ models. For photons, the code accounts for incoherent and coherent scattering, the possibility of fluorescent emission after photoelectric absorption, absorption by pair production with local emission of annihilation radiation, and bremsstrahlung. A multi-scattering model is used for electron transport that includes positrons, k x-rays, and bremsstrahlung but does not include external or self-induced fields.

Important standard features that make MCNP very versatile and easy to use include a powerful general source, criticality source, and surface source; both geometry and output tally plotters; a rich collection of variance reduction techniques; a flexible tally structure; and an extensive collection of cross-section data.

MCNP contains numerous tallies: surface current & flux, volume flux (track length), point or ring detectors, particle heating, fission heating, pulse height tally for energy or charge deposition, mesh tallies, and radiography tallies.

The MCNP code is developed and maintained by Los Alamos National Laboratory simulation group.

This code is widely used and main specific areas of application include following:

- radiation protection and dosimetry
- radiation shielding, radiography, medical physics
- nuclear criticality safety
- detector design and analysis
- accelerator target design
- fission and fusion reactor design
- decontamination and decommissioning

6. The FISPACT code.

FISPACT is an inventory code that was included in the European Activation System[1] [9]. The code has been developed for activation calculations for materials used in the fusion fields[2] [10]. It is able to give information about atomic density and activity of a material irradiated with neutrons or charged particles. It takes its origins from FISPIN, an activation code used for fission reactors [10]. There are several (about ten) versions of the code starting from Version 1 through Version 2007. The code uses external libraries of all cross sections and decay data for the most important nuclides that play a key role in the neutron flux irradiation. The output of the code gives information about the activity (Bq), the amount of nuclides (in atoms and grams) and also the γ-dose rate (Sv/h). FISPACT works with one energy group cross sections so it requires the collapsing of the library with the neutron spectrum [10].

The EAF[3] libraries[11] cover an energy range from thermal to 60 MeV. The code can calculate the effects of irradiation of different minor actinides. It have to be considered that the EAF libraries contain infinite dilution cross sections; this means that, if the actinides is present in significant proportion in the material, the output data won't be representative because the code doesn't include self-shielding and burn-up effects [10]. However, the calculation of a pure actinide is possible to model fuel in a fission power station or in a transmutation system, but the results won't be as exact as a dedicated fission reactor code such as FISPIN. To perform a calculation many data files are required

FILES file contains all the information about the location of all files requested for running the code; it must be located in the same directory of the FISPACT executable. The fundamental information that are necessary to write an input in FISPACT are: material details that has to be irradiated, time of irradiation and decay time after which evaluate the activity, specific information about the value of the neutron flux and the neutron spectrum that will be used [10]. The input is composed by a series of words that allow to perform different actions; these words can be divided in two categories:

- **preliminary code words**: they are concerned with library specifications;

---

[1] EASY: it is an international standard for simulation of activation, transmutation processes and radiation damages caused by nuclear reactions and decays. It is developed by the United Kingdom Atomic Energy Authority at Culham.
[2] It has been adopted by the ITER project as the reference activation code.
[3] The European Activation File (EAF) is an extensive data library prepared for the European Activation System (EASY). The EAF-2010 activation-transmutation neutron nuclear data library includes 816 target isotopes.

- **main code words**: they gives details about the materials composition and the irradiation history.

Usually, these words are used following the chronological order of the neutron irradiation. It is possible to create irradiation routines that can be repeated in loop to simulate, for example, a one week irradiation program. The input file describes also the required type of output. A typical output consists of a first part that reports preliminary information such as the name of the program, its version and library information. This part is then followed by the nuclide inventory that is reported for each time interval specified in the input. The standard output table gives information about the composition in atoms, the mass (g), the activity (Bq), the α, β, and γ energy and different type of γ-dose (Sv/h).

7. ERANOS model and preliminary results.

The preliminary neutronic analysis of the reactor was carried out to better evaluate the irradiation feasibility.
The model of the system, developed using the RZ geometry, allows to give more importance to the core, but this leads to less precision on the shield because it is spherical. The ERANOS model is shown in Figure 3:
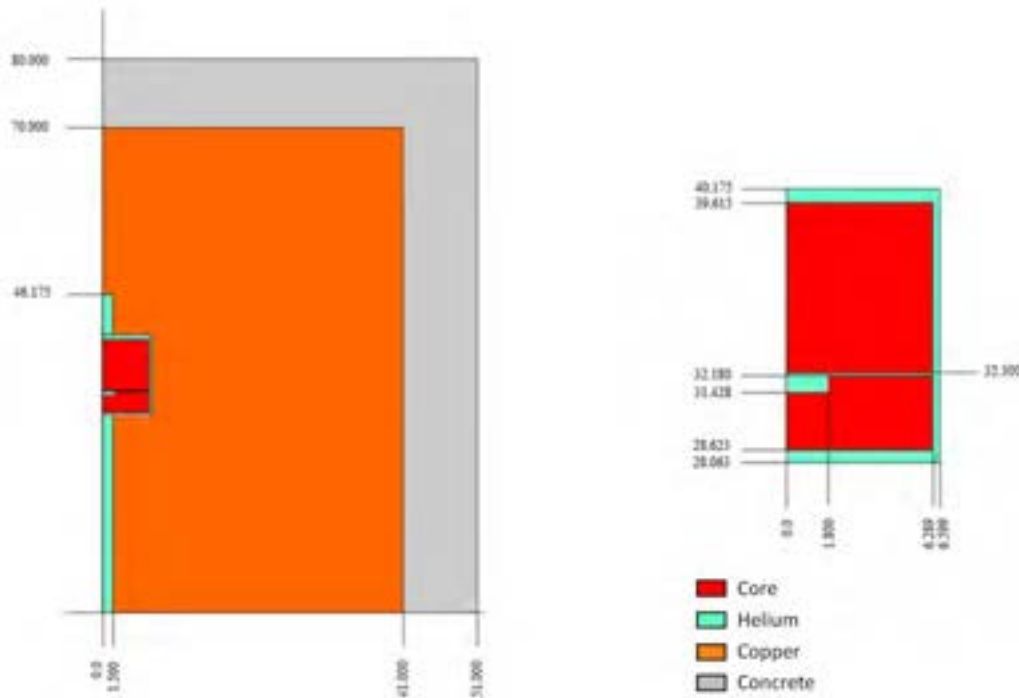
Figure 3 - ERANOS model of TAPIRO (dimensions in cm, the image is not in scale).

As it can be noticed in Figure 3, only 50 cm of the concrete shield were considered (instead 175 cm); the reason of this choice is that the calculation goals are referred to the internal part of the system, above all the core and the reflector. After a preliminary check, it was possible to evaluate a negligible change between the two configurations, even the multiplication factor remains constant. Moreover, the

calculation time for the accurate geometry was extended of a factor 10. As showed in the same figure, the cooling channel between the core and the reflector (for upper, lower and external interfaces), is filled with coolant (He). In this position, near the core axis, there is a cavity; this is realized to allow the insertion of the shim pellet. The use of this pellet is useful to create the condition of minimum critical mass (M.C.M) relative to the first criticality of the reactor [2]. The configuration used in the calculations performed by ERANOS is the operative critical mass (M.C.O) without the shim pellet. In the M.C.O. configuration the cavity is filled with helium.

At first, two different energy structures, 33 and 172, have been considered to analyze the influence on the k_{eff} value of different energetic structures. The reactivity calculation has been carried out solving the transport equation using different S_n approximations; in particular S_4, S_8 and S_{16}Gaussianequadratures. This method is implemented in BISTRO module inside ERANOS and it is more accurate in comparison with the diffusion method. Obviously, this one is more simple to solve and it requires less computational resources than the other but, in some region of the spectrum, the given solution is not enough precise. For 33 energy groups and S_4 approximation, a preliminary calculation has been performed with two different reference libraries: ENDFB-6.8 and JEFF-3.1 to check the influences of the reference data (Table2):

	k_{eff}	
$33G\_P_0\_S_4$	ENDFB-6.8	JEFF-3.1
Transport	1.02923	1.02925

Table 2 - k_{eff} comparison for diffusion and transport theory

Once defined the calculation mode and the reference library the reactivity calculation results depend on the $P_n$approximation used in ECCO for the determination of the cross sections, from the S_n approximation chosen in BISTRO and also from the energy grid used. The reactivity calculation results are shown in the following tables. Each table is relative to a different value of the discrete ordinate (4, 8, 16) and the k_{eff} values are submitted for different P_n approximations and energy groups.

	k_{eff}	
S_4	33 energy groups	172 energy groups
P_0	1.02925	1.02784
P_1	1.0161	1.01471
P_3	1.02237	1.02086

Table 3 - k_{eff} comparison with N=4

	k_{eff}	
S_8	33 energy groups	172 energy groups
P_0	1.02662	1.02521
P_1	1.01286	1.01145
P_3	1.01972	1.0182

Table 4 - k_{eff} comparison with N=8

	k_{eff}	
S_{16}	33 energy groups	172 energy groups
P_0	1.02602	1.02461
P_1	1.0124	1.01097
P_3	1.01921	1.01767

Table 5 - k_{eff} comparison with N=16

In Tables 3-5 it can be noticed that the k_{eff} values decrease towards the critical condition according with the increase of the calculations accuracy. However, the increase of the accuracy needs more computational resources and so the calculation time grows up.

The results shows that the increasing of S_n, from 4 to 16, and correspondingly the degree of the P_n polynomial allow a more accurate analysis of this small system where leakage and neutron scattering has an important effect. About the different energy structures analyzed, even if for a fast reactor the standard 33 energy grid is used, the results obtained with 172 energy groups have be chosen to have a more fine characterization of the neutron spectrum up to the biological shield and to better carry on in the minor actinides analysis. About P_n approximation another important evidence is that P_1 approximation is not suitable because the basic transport equation solved in this case is characterized by terms that not allow to take into account important information about the neutron transport phenomenon. Corrected P_0 and P_3 are much better, in both cases the results are very closed, so to carry on the next analysis the P_0 corrected results are chosen.

About the value of the discrete ordinates, it can be said that the best choice is represented by the S_{16} approximation because of the cylindrical shape of the core; this value of the angular ordinate ensures a more accurate calculation.

After this considerations all the other calculations and analysis have been carried out with 172 energy group structure, corrected P_0 and S_{16} discrete ordinates approximations.

The reference k_{eff} is equal to 1.02461 and the reactivity of the system is:

$$\rho = \frac{K_{eff} - 1}{K_{eff}} = 2402 \, pcm$$

A first set of runs by Serpent code has been executed to estimate the keff values with the control rods in completely inserted, with the TAPIRO core maintained at room temperature.

8. Serpent model and preliminary results.

The Serpent code uses a universe-based geometry model for describing complicated structures, very similar to MCNP. This means that the geometry can be divided into separate levels, which are all constructed independently and nested one inside the other.

Values for geometry are taken from MCNP model of TAPIRO, with some differences. Reactor core, inner and outer reflector are faithfully reproduced, such as diametral, tangential, and radial 1 irradiation channels. Conversely radial channel 2 and source channel can't be represented with the version used serpent (1.1.19), because they are not parallel to any axis (this option has been inserted in serpent 2).

The TAPIRO control system is based on the regulation of the neutron escape from core. For this purpose, five copper cylindrical rods have been located in the inner reflector. Each of the rods can be withdrawn for a total axial length of 15 cm creating a void region of the same length in the reflector.

In their withdrawal, the rods go down into apposite cavities in the lower part of the inner reflector. Two control rods of 7.5 cm of diameter are used as safety rods (SR1 and SR2) since they realize the greater negative reactivity insertion of the rods set. Safety rods are maintained completely inserted during normal operation and used for normal shutdown or for SCRAM. Two shim rods of 5.7 cm of diameter ensure the reactor rise to power (S1 and S2).

The fine adjustment of the criticality is obtained by the regulating rod. All results showed lately in this work has been obtained with all rods completely inserted, in order to have the highest possible value of neutron flux.

A further simplification compared to the real geometry of the research reactor is the representation as a regular parallelepiped of the part of concrete that surrounds the thermal column. This was possible because the region has a null neutronic relevance, so doesn't influence the aim of this work.

There are several ways that Serpent uses to calculate k_{eff}. The analog estimate looks at the entire geometry, while the implicit estimate is calculated only in the universe set by the user. In addition the eigenvalue can be calculated using the collision estimate or the absorption estimate, that take into account different type of interaction between neutron and matter, and through which can be also calculated k_{∞}(Table 6) .

Parameter	Description	Value	Relative error
ANA KEFF	Analog estimate of k_{eff}	1.01844	1.30E-05
IMP KEFF	Implicit estimate of k_{eff}	1.01842	1.00E-05
COL KEFF	Collision estimate of k_{eff}	1.01843	1.00E-05
ABS KEFF	Absorption estimate of k_{eff}	1.01842	1.00E-05
ABS KEFF	Absorption estimate of k_{∞}	1.02508	1.00E-05

Table 6 - k_{eff} Serpent results

9. MCNP model

The TAPIRO model implemented in MCNP code is the standard reference modelutilized for reactor operation and experiment modelling. It is actually constructed through surface-based cell volumes allowing a complete domain representation of both reactor core, reflector and irradiation channels.

The core is composed of a number of fuel cylindrical plates cooled by helium and a calibration pellet. The central part of the diametral channel is filled by radially oriented pellets as well.

The MCNP results presented here are obtained without the calibration pellet and with the central pellets inserted. In addition, the Safety Rods (SR1 and SR2) and Shim Rods (S1 and S2) are considered inserted.

Considered irradiation channels are the diametral channel, tangential channel and radial channel 1. They are all filled with air and the copper plugs are also removed.

Nuclear data library utilized is JEFF3-1 provided by NEA Data Bank and processed at 300 K.

Model normalization is made at the flux peak according to standard reference [12].

Diametral channel characterization is obtained through flux evaluation and minor actinides fission and capture reaction rate. This is performed with the mesh tally MCNP feature through which a mesh is superimposed over the actual geometry to obtain the response in a customized calculation grid.

Preliminary results reported in this document constitute a first evaluation of requested quantities. Further optimized simulations are needed to compare long-running analog calculations and possible optimized variance reduction techniques.

The flux in the diametral channel and the fission reaction rates for all minor actinides are reported. Relative errors are mostly below 5%. By contrast Pu239 exhibits errors up to 33%-60% as depicted in error bars within the plot Figure 14 – ^{239Pu} fission rate in the diametrical channel. In addition, Cm244 and Cm245 errors far from reactor core – namely in the external part of the reflector towards the shield – are as high as 12%-33% and 10%-34% respectively. Work reported in the future will include the same results with acceptable statistical uncertainties.

Within the present report, absorption reaction rates are not showed – as well as averaged absorption reaction rates – since stochastic errors are too high and Monte Carlo simulations require further optimizations.

10. Fluxes and reaction rates.

For the 172 energy groups, an energy integrated flux traverse, along one of the TAPIRO experimental channels (the diametrical one), has been shown in Figure 4, for both ERANOS and Serpent codes.

As diametral channel has the axis parallel to y-axis, this axis has been divided into 220 parts, one for centimeter, while on the XZ plane the mesh forms a square of 0.4 cm side. So each detector has a volume of 0.16 cm^3. As showed in Figure 4 the neutron flux decrease rapidly outside the core, and became negligible outside the copper reflector, where few neutrons arrive, with a consequently increase of the statistical error of Monte Carlo calculations. The absence of neutron after the reflector is due to massive absorption of borated concrete.

Considering these issues and that for an irradiation problem must be used the highest possible value of flux, from now will be considered only the internal part of the diametral channel, from the core center until y = 50 cm.
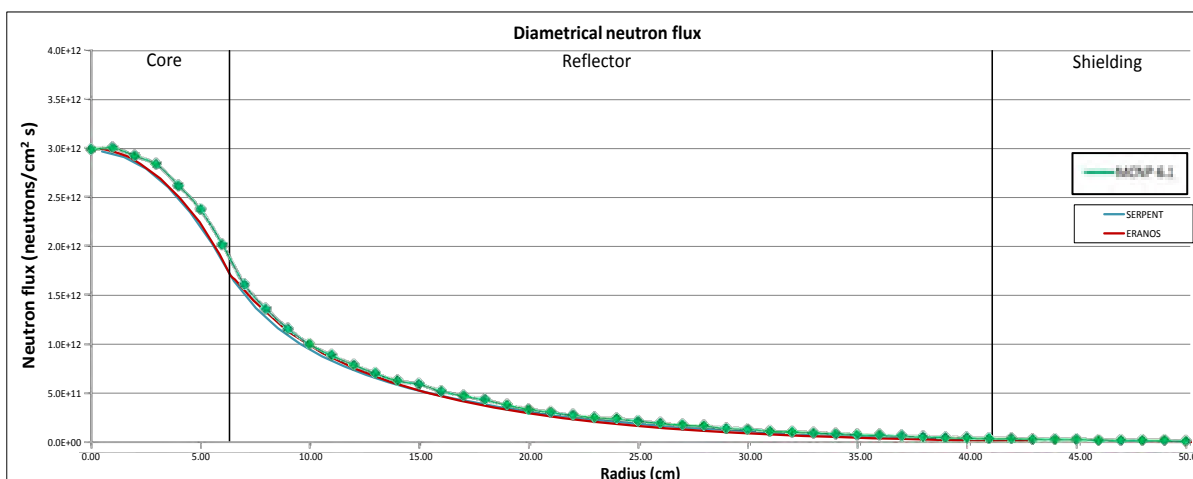
Figure 4- Diametrical neutron flux comparison at 5 kW.

The highest value of the neutron flux is 3.00 x 10^{12} [n/cm^{2}s] [12], obtained in the centre of the core. The overall trend decreases moving from the core trough the shield with an important reduction at the interface core/reflector.

It is evident in the Figure 4 that there is a good agreement between the two codes; the total flux is characterized by the same trend and, as expected, by the same values in all the positions of the diametrical channel. Conversely, MCNP simulations show some minor discrepancies within the reactor core. Error bars are reported in the figure, even if small compared to plot scale.

The neutron flux expressed for energy groups is known as the neutron spectrum, this can be analyzed in different position in the reactor to evaluate the neutron balance and the neutron energy transition in the system. In this work the neutron spectrum has been determined in different position inside TAPIRO, among the diametrical channel to characterized this experimental channel and to choose the minor actinides samples position. The spectra analyzed are in the central part of the core, close to the boundary of the fuel, at the beginning of the reflector, in a position of the diametrical channel equivalent to the tangential channel distance, in the middle of the reflector and also in the middle of the shield.

The spectrum of TAPIRO in the centre of the core is shown in Figure 5 :
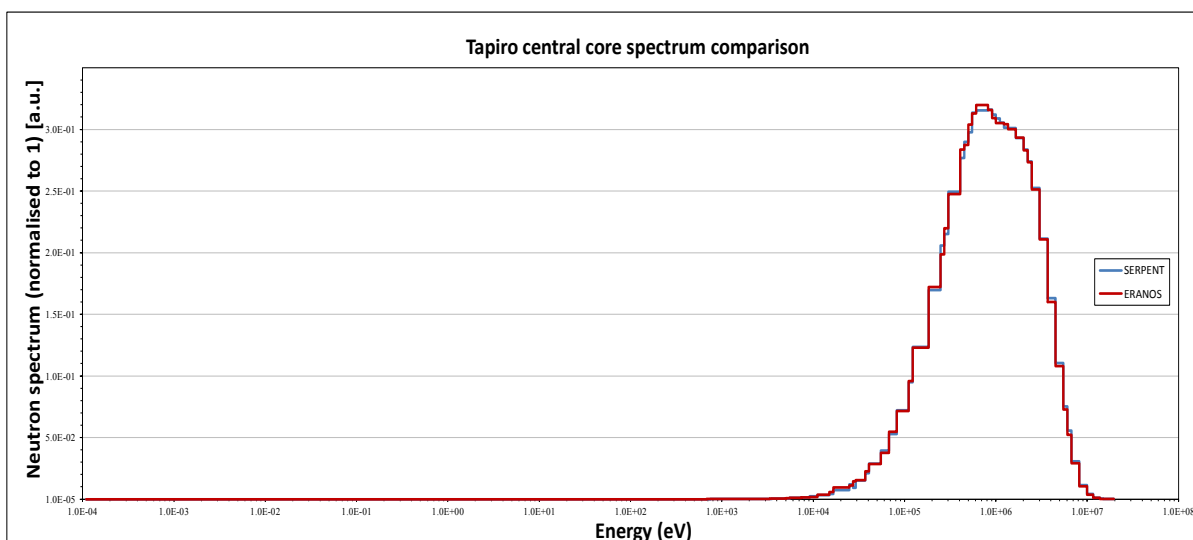
Figure 5- TAPIRO central core spectrum comparison

The spectrum in Figure 5 with a peak around 820 keV, is a typical fission spectrum, this is a peculiarity of this reactor; for this reason TAPIRO is a unique reactor that can be used for calibration scopes. The Figure 5 shows an almost perfect coincidence of the neutron spectrum in the central part of the core, although the two codes have a different transport solution method.

The neutron spectrum evaluated in other positions of the system are shown in Figure 6-8 :
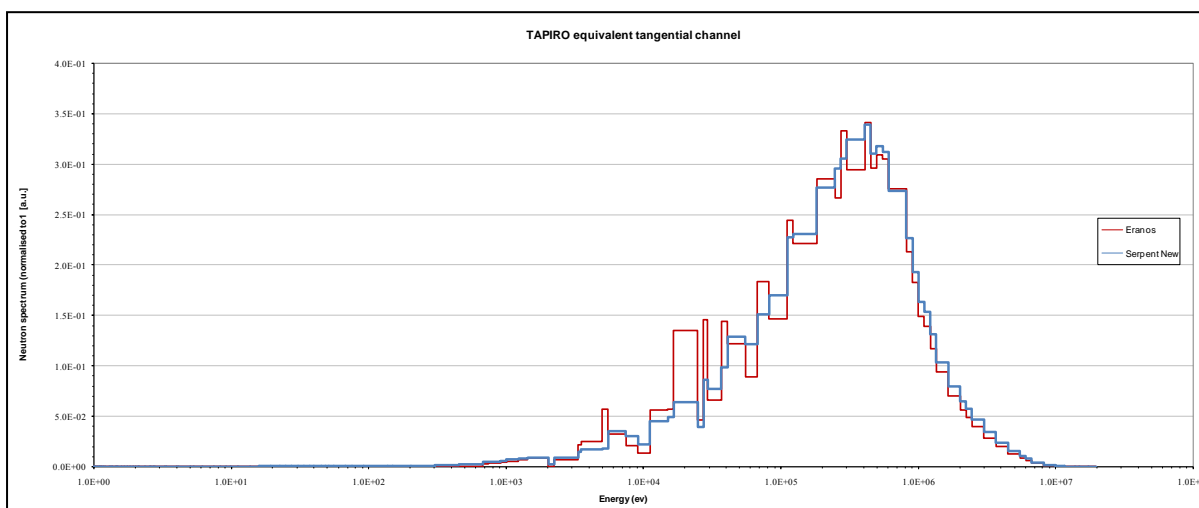
Figure 6- TAPIRO neutron spectrum in the equivalent tangential channel

The spectrum in the equivalent tangential channel position (Figure 6) shows a neutron transition from higher to epithermal energy, this is due to the neutron scattering in the copper reflector. In this case the neutron peak is near 450 keV.
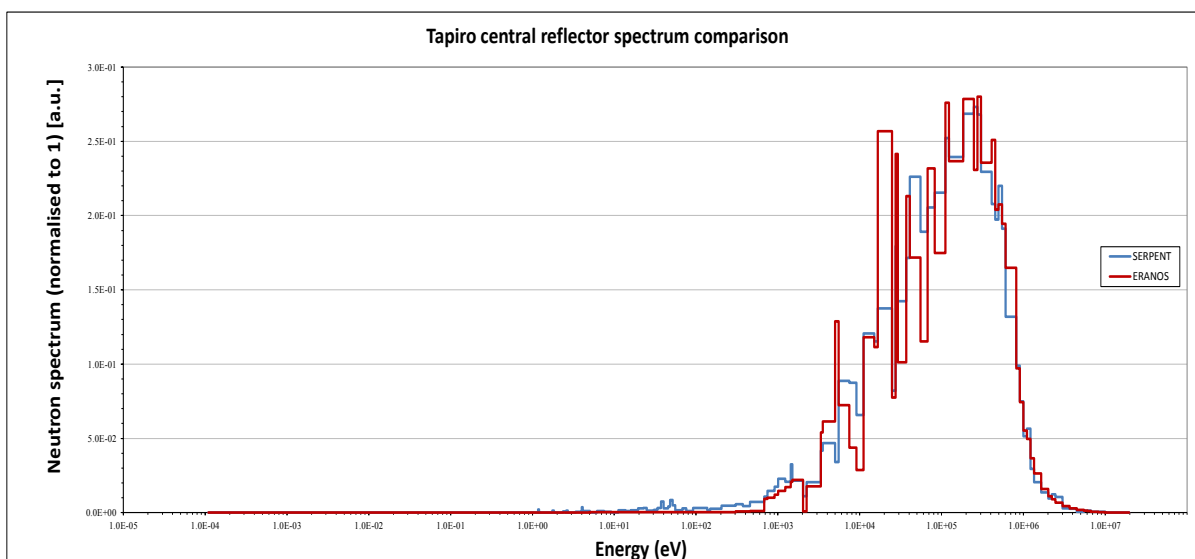
Figure 7 - TAPIRO central reflector spectrum comparison

The spectrum in the reflector center, Figure 7, has the same characteristic of the previous one, in this case the peak is near 300 keV. Figure 7 is still characterized by a good agreement with some differences due to the different geometry description, more accurate in SERPENT, where the influence of different materials and their interfaces is more dominant than in ERANOS, and even for the statistical influences that affected SERPENT.
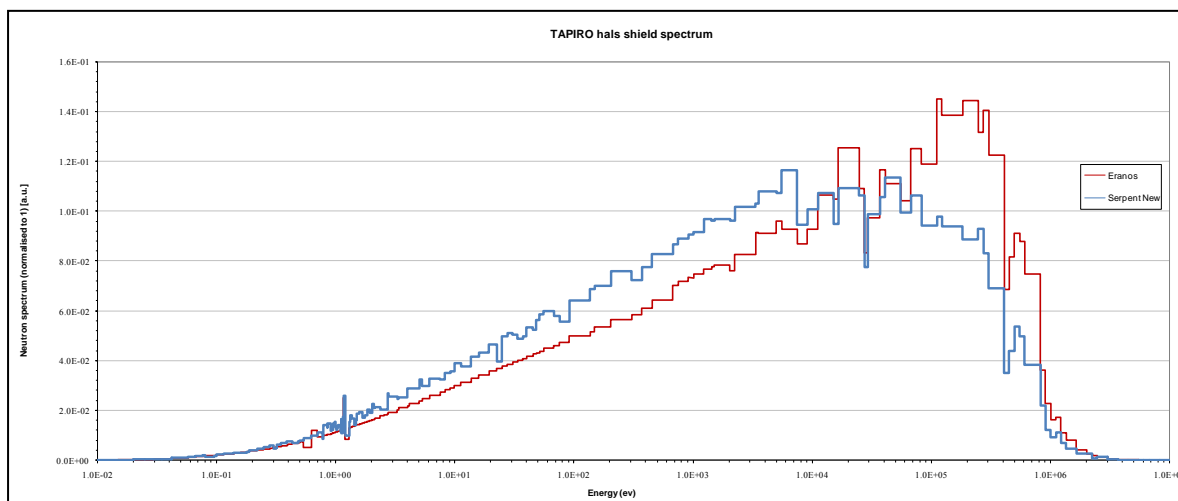
Figure 8- TAPIRO neutron spectrum in the middle of the shield

In the last spectra position, in shield center (Figure 8), it can be noticed that the neutron spectrum in the selected points of the diametrical channel is characterized by a progressive transition from a nearly fission spectrum in the in core position of the channel to a progressive softening moving to peripheral positions. The thermal neutron population that is negligible at core center progressively growth with the detector distance from the core axis.

This is evident by the growth of the curve at lower energies, in this case the spectrum has a peak near 250 keV.

Another important aspect to analyze the importance of the fast, epithermal and thermal flux in the whole system is the evaluation of the neutron flux distribution in four macro-energy zones. The choice of these four macro zones has been finalized to the analysis of the neutron spectrum in relation to the possibility to evaluate the behavior of different minor actinides, considering in the following paragraphs, in the various positions of the system.

Then a comparison between the neutron flux distribution in the four macro-energy zones can be done:
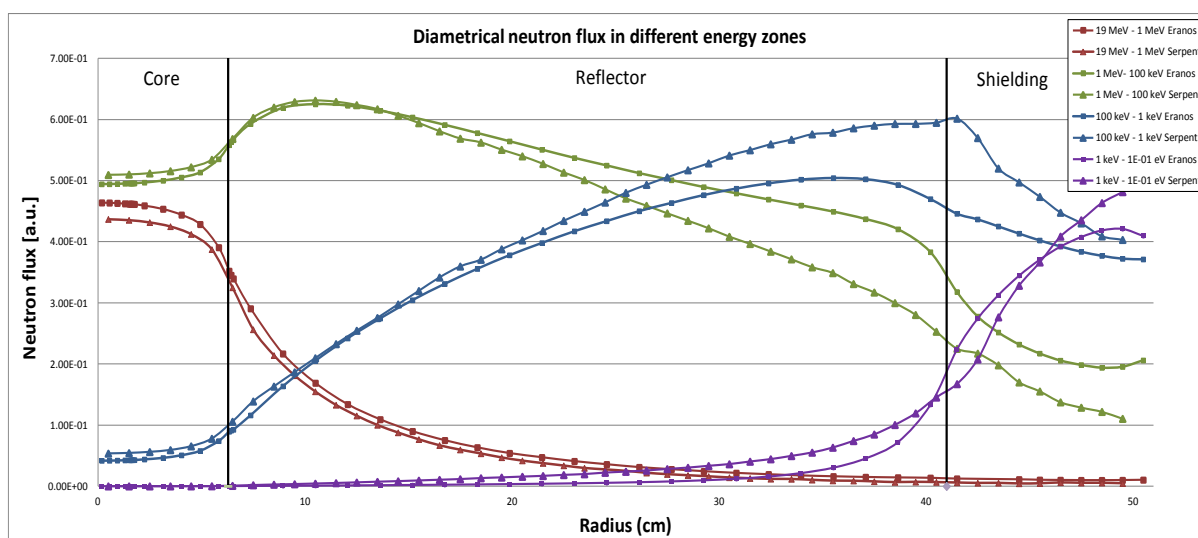
Figure 9 - Flux in macro energy zones comparison

The trend shows in Figure 9 for both calculation codes is very similar. Figure 9 shows the predominance of the flux between 1 MeV and 100 keV till the second half of the reflector, where the epithermal flux (100 keV - 1 keV) become dominant. The thermal flux (1 keV - 0.1 eV) is important just in the last part of the shield due to the presence of light nuclides. The high energy flux (19 MeV - 1 MeV) is significant in the core where many high energy neutrons are generated from the fissions, and just a little bit in the first part of the reflector. The only noticeable difference can be found in the energy group between 1 MeV and 1 keV, but only after the middle of the reflector. This differences can be justified with the presence of some interfaces in the geometry used for SERPENT, interfaces that causes a decrease of the number of neutrons with energy between 1 MeV and 100 keV due to scattering.

These comparisons allow to conclude that the results of the flux calculation obtained with ERANOS can be considered very reliable.

A reaction rate is defined as the product between the macroscopic cross section that characterize a particular reaction and the neutron flux. It expresses the number of reactions per unit time (1/s):

$$R(\vec{r}) = < \sigma(\vec{r}, E)\phi(\vec{r}, E) >_E$$

Where the $<>_E$ represents the integration over energy. These information are very important to describe the behavior of different actinides relative to the fission and capture reactions, in different position of TAPIRO. The minor actinides that have been considered in this work are a small part of those that were

used in an experiment performed in the U.S. at INL (Idaho National Laboratory) [13]. These minor actinides are shown in Table 6:

Uranium	Plutonium	Neptunium	Americium	Curium
^{235}U	^{239}Pu	^{237}Np	^{241}Am	^{243}Cm
^{238}U	^{241}Pu	/	^{243}Am	^{244}Cm
/	^{242}Pu	/	/	^{245}Cm

Table 7 - Minor actinides chosen for a preliminary analysis in TAPIRO

Thanks to the previous flux calculation, it was possible to determine the fission and the capture reaction rates for all the tabled minor actinides, along the diametrical channel of TAPIRO, these are shown in Figures 10-31.
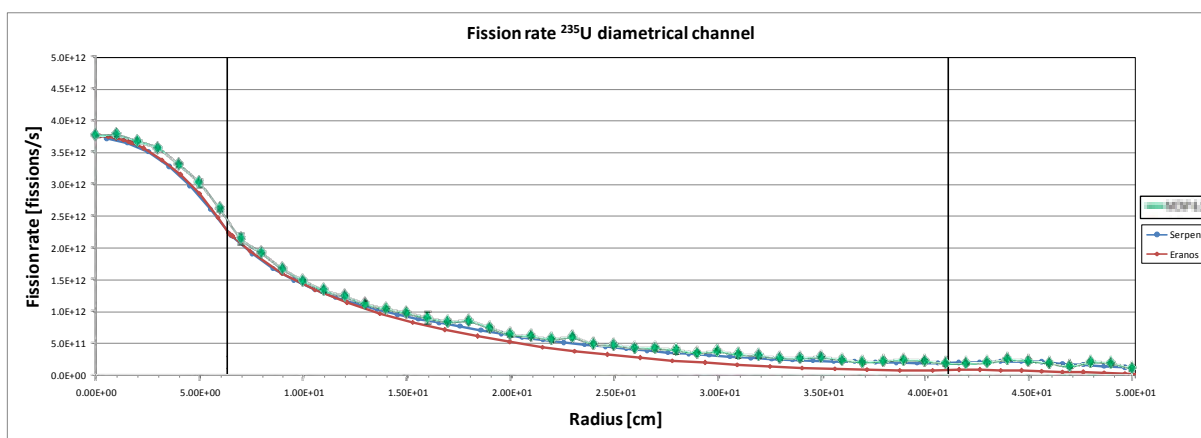
Figure 10 - ^{235}U fission rate in the diametrical channel.
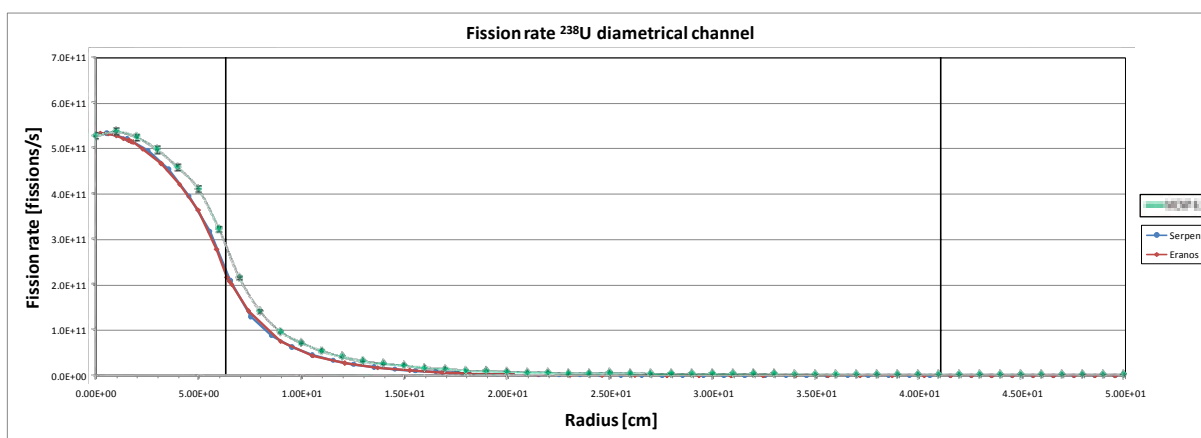
Figure 11 - ^{238}U fission rate in the diametrical channel.
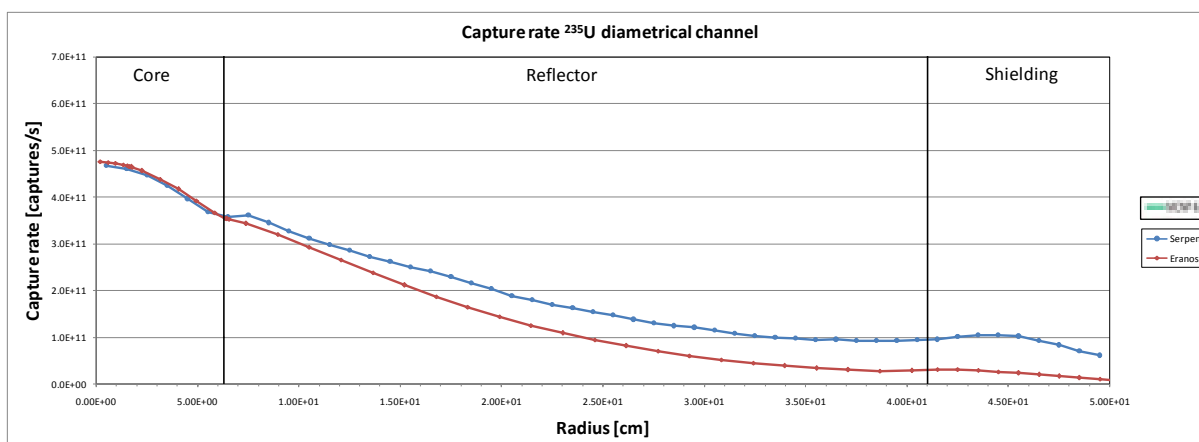
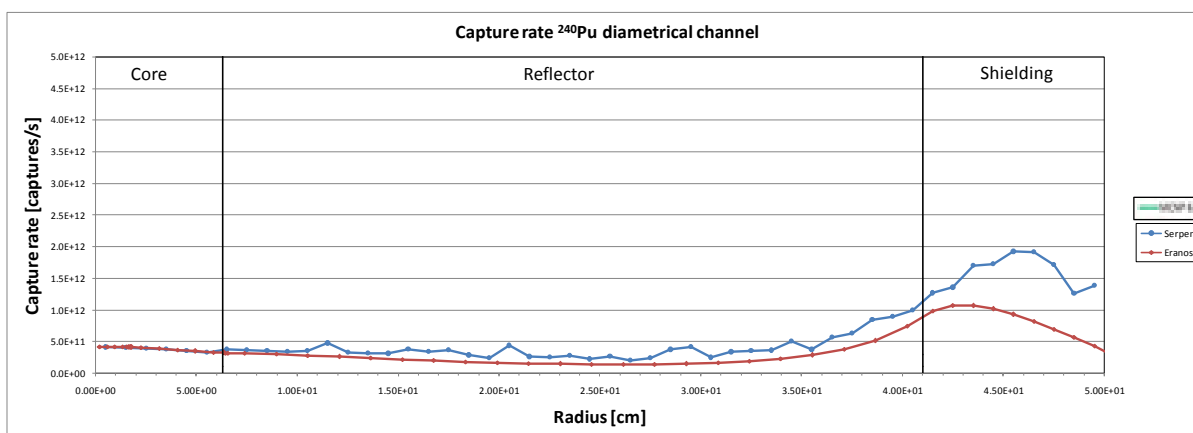**Figure 12 - ^{235}U capture rate in the diametrical channel.**
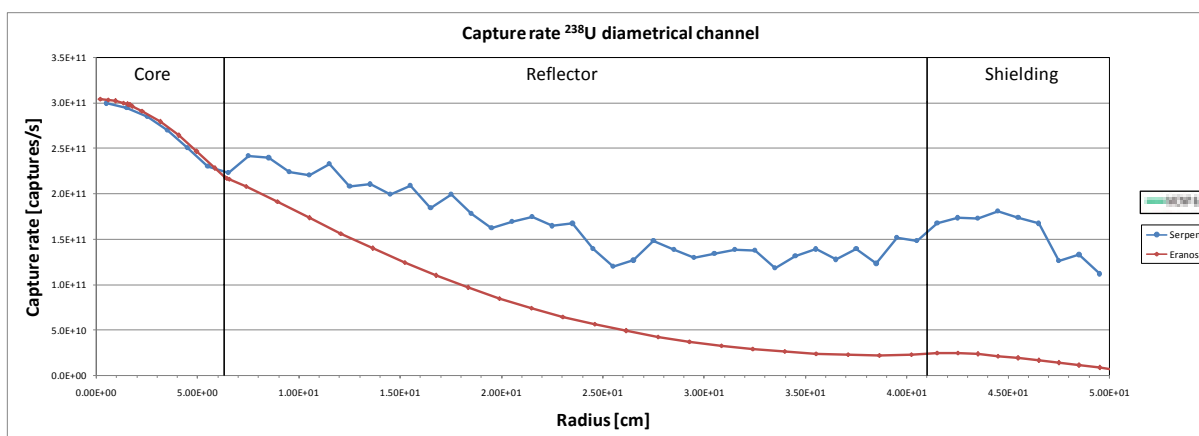
Figure 13 - ^{238}U capture rate in the diametrical channel.

The two isotopes of uranium considered have a similar trend (Figures Figure 10-13), about the shape of the curve. ^{235}U is higher than ^{238}U both for capture and fission rates, and the maximum value is located in the centre of the core. ^{235}U (Figure 10), as expected from a fissile isotope, is capable of sustaining nuclear fission with neutrons of any energy. As expected from flux traverse behavior, fission rate is higher in core center, but has a relative maximum near the end of reflector, where the number of thermal and epithermal neutron begin to be consistent. ^{238}U is practically insensitive to thermal neutron, while has a great affinity with fast fissions, so its fission rate (Figure 11) is more regular and narrow and about one order of magnitude lower than ^{235}U. Capture reaction rates have a behavior less regular, with a little relative maximum just out of the core, probably due to scattering into inconel, and a bigger maximum at the end of outer reflector. The second peak is particularly evident in ^{238}U capture rate (Figure 13) only for the Serpent estimation.

The differences between the two codes are negligible inside the core and then gradually increase moving to the reflector and the shield. Obviously, these differences depend on the different value of the cross sections of the two isotopes, of the geometry description, fluxes evaluation and of the Serpent statistic.

In all Serpent simulations relative errors are contained in the range between 0.6% and 25%, as conversely showed in Monte Carlo simulation. Obviously the highest dispersion for all isotopes reaction rates are located in the last few points at the extremities of the traverses. The results are

compatible with the estimated neutron flux traverse, since value of reaction rates in a point is never greater than flux value in the same point.

MCNP simulations exhibit a good agreement for 235U even taking into account the relative errors reported in the plot. By contrast, 238U fission reaction rates are different even taking into account for the error gaps. Error bars are reported in the figure.
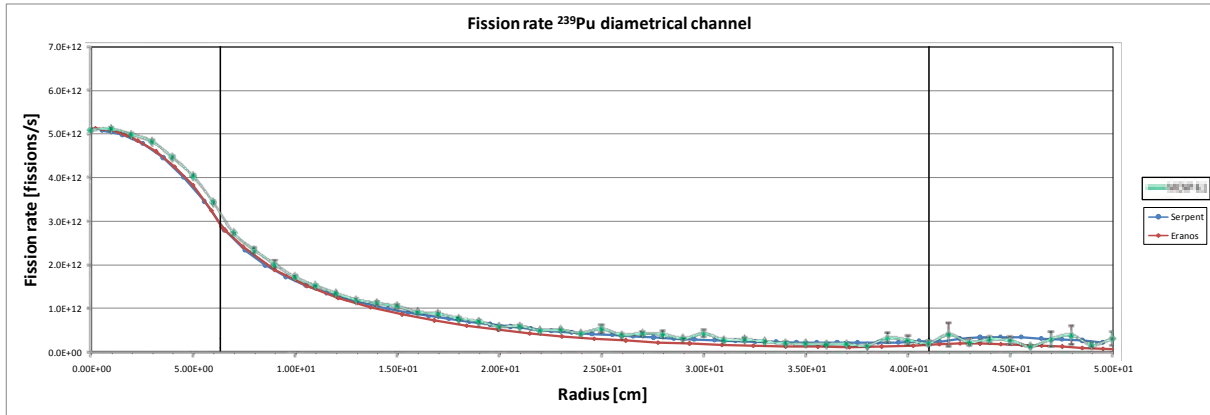
Figure 14 – ^{239}Pu fission rate in the diametrical channel.
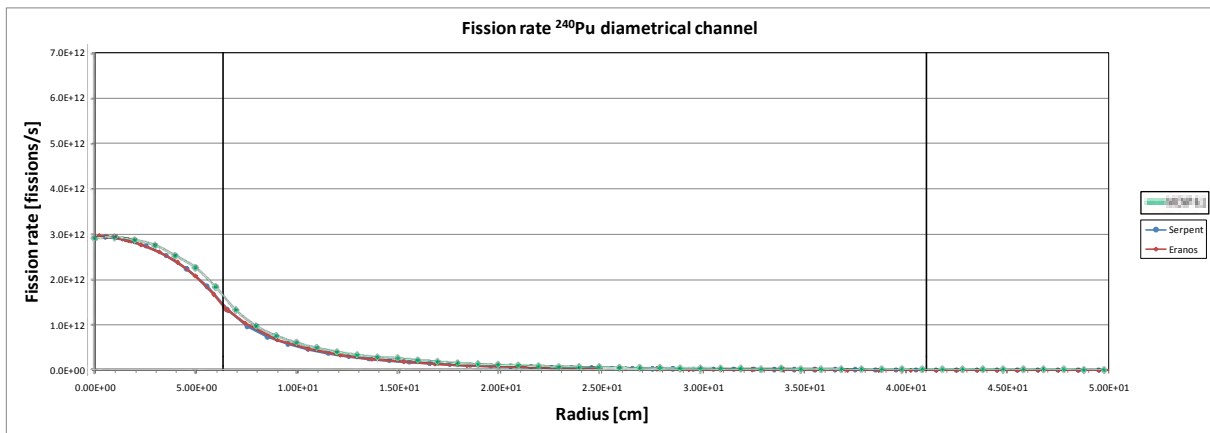
Figure 15 – ^{240}Pu fission rate in the diametrical channel.
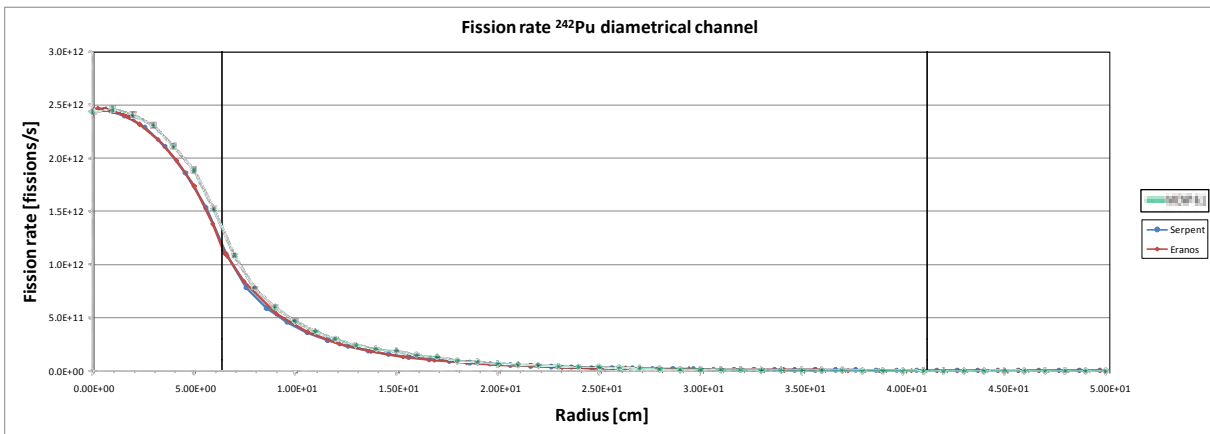
Figure 16 – ^{242}Pu fission rate in the diametrical channel.
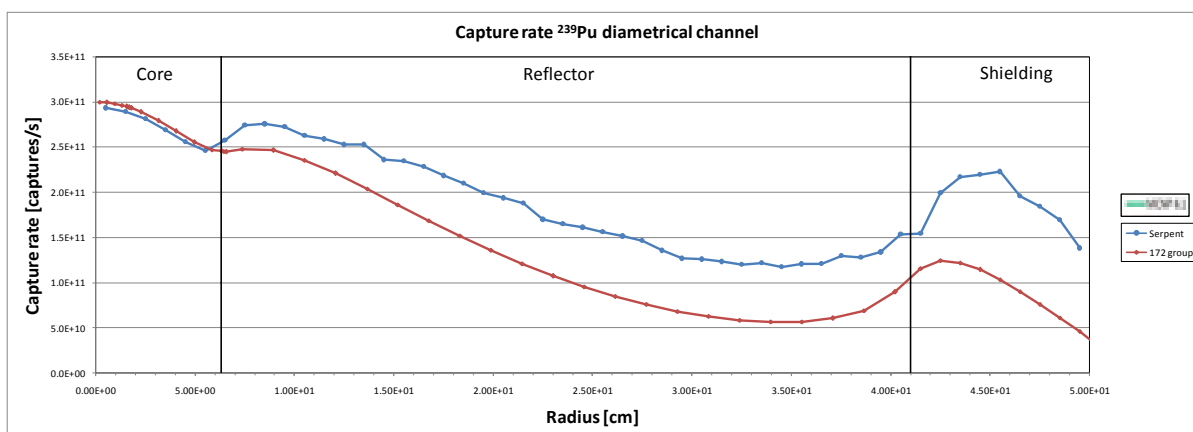
Figure 17 – ²³⁹Pu capture rate in the diametrical channel.

Figure 18 – ²⁴⁰Pu capture rate in the diametrical channel.
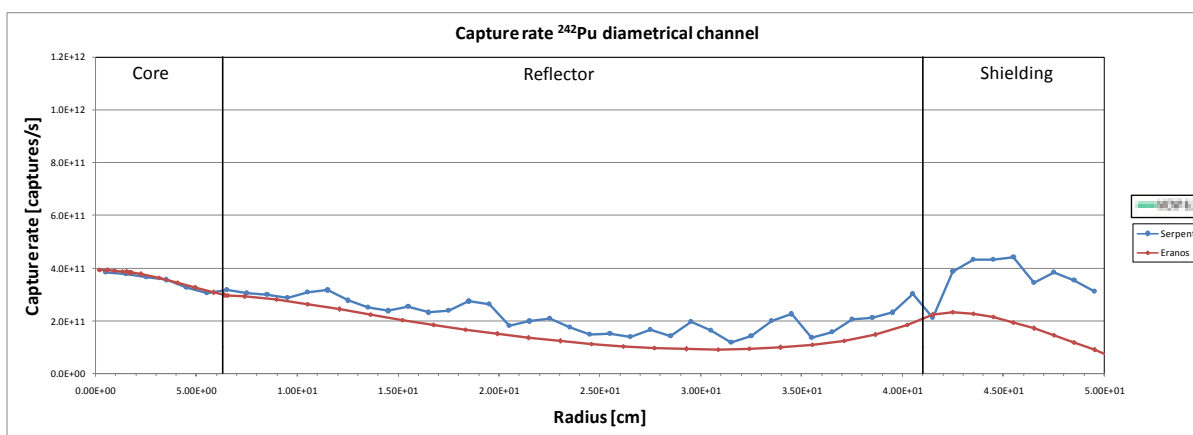
Figure 19 – ²⁴²Pu capture rate in the diametrical channel.

Regarding plutonium, has been considered three isotopes, ²³⁹Pu, largely produced in nuclear plants from absorption of ²³⁸U and often used in nuclear weapons, that represent about 0.8% of spent nuclear fuel and has an half-life of 24100 years, ²⁴⁰Pu, a fertile isotopes produced by absorption from ²³⁹Pu, with an half-life of 6563 years, and ²⁴²Pu, an isotopes of plutonium with low radioactivity, about 15 times less than ²³⁹Pu, but the second longest lived, with an half-life of 373300 years.

For the fission rates (Figures 14-16), it is possible to see a trend similar to the uranium isotopes. The fissions of the ^{239}Pu are more evident in the core respect to the other, this is a fissile isotope.

The MCNP comparison shows a deviation in the core-reflector region. Error gaps are reported in the figure, even if small compared to plot scale.

Instead, the capture rates (Figures 17-19) is completely different; the decrease moving away from the core is lighter and in the second part of the reflector, the reaction rate start to increase reaching a peak just after the shield interface and then goes down very quickly, thanks to the rapid reduction of the neutron flux. This phenomenon is more evident for ^{240}Pu whose peak is one order of magnitude bigger than the peaks of the other two isotopes. It is important to notice that for ^{240}Pu this peak is higher than the value reached inside the core.

For the fission rates two codes are in completely harmony instead of capture rates where the differences are evident, especially in ^{239}Pu capture rate.
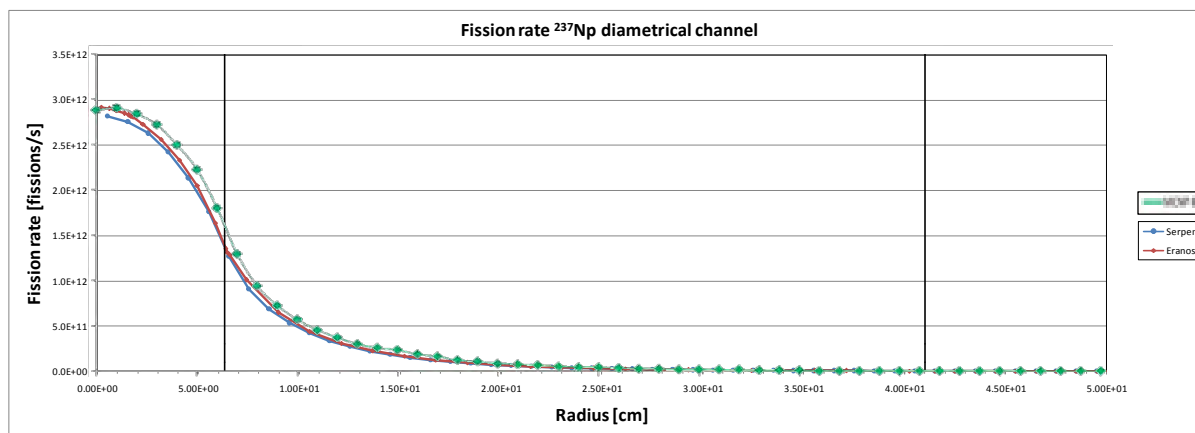
Figure 20 – ^{237}Np fission rate in the diametrical channel.
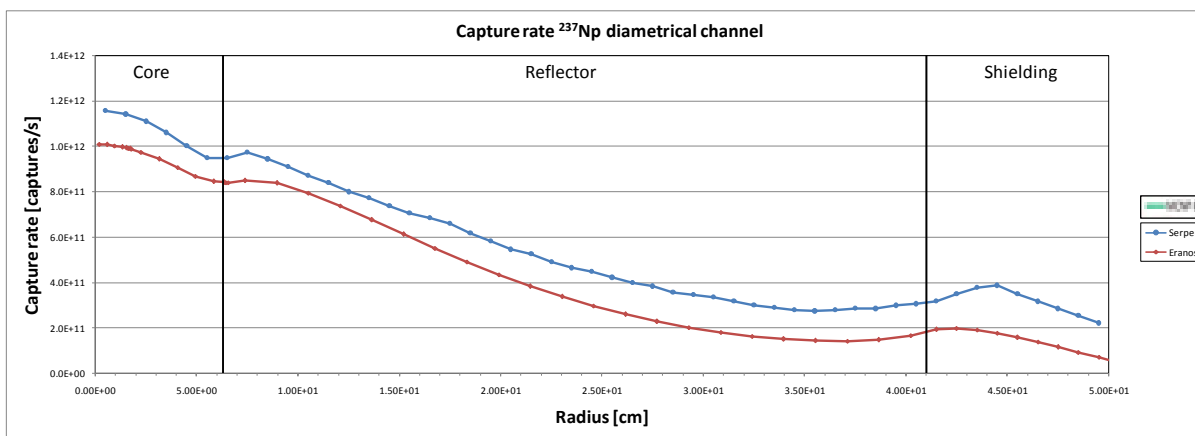
Figure 21 – ^{237}Np capture rate in the diametrical channel.

First of minor actinides taken into account is neptunium, and precisely its most stable isotope, ^{237}Np, with an half-life of $2.14 \cdot 10^6$ years. It is the only neptunium isotope produced in significant quantity in the nuclear fuel cycle, both by successive neutron capture by ^{235}U (which fissions most but not all of the time) and ^{237}U, or (n,2n) reactions where a fast neutron occasionally knocks a neutron loose from ^{238}U or isotopes of plutonium. ^{237}Np also formed into spent nuclear fuel as the decay product of ^{241}Am, but it happens only on long period.

Even if [237]Np is predicted to be fissile, like other odd isotopes, its fissionability has been experimentally showed [14]. This justify the behavior of fission reaction rate (Figure 20), similar to fissionable isotopes, while capture reaction rates has two relatives maximum coincident with the begin and the end of the reflector (Figure 21).

It can be noticed that near the interfaces between the core and the reflector, and the core and the shield there are small and rapid variations of the reaction rates. The reason is the interface effect that affects a deterministic calculation system like ERANOS. This effect occurs also in the other isotopes but in some cases is less evident.

Relatives errors are between 0.4% into the core and 6% into the external points of diametral channel.

In the capture cross section there is an evident Serpent overestimation among whole channel instead of the perfect overlapping between both codes.

MCNP exhibits the same trend in overestimating the reaction rates for [237]Np within the central core-reflector region. Error bars are reported in the figure, even if small compared to plot scale.

Most common and stable isotopes of americium, [241]Am and [243]Am, has been selected to be simulated. [241]Am,with half lives of 432.2 years, derives from decays of some isotopes of plutonium ([241]Pu), curium ([241]Cm) and berkelium, while [243]Am, with half-life of 7370 years, derives mainly from [242m]Am or [243]Pu in nuclear fuel cycle.

For americium isotopes 241 and 243 shown in Figures 22-25 it is possible to see a decreasing trend from the centre of the core, with a small peak at the beginning of the shield for the capture rate. An important consideration is that for americium, and also for neptunium, the reaction rates are of the same order of magnitude, differently from the case of uranium, plutonium and also curium, as shown in Figures 20-21, where the fission rate is bigger.
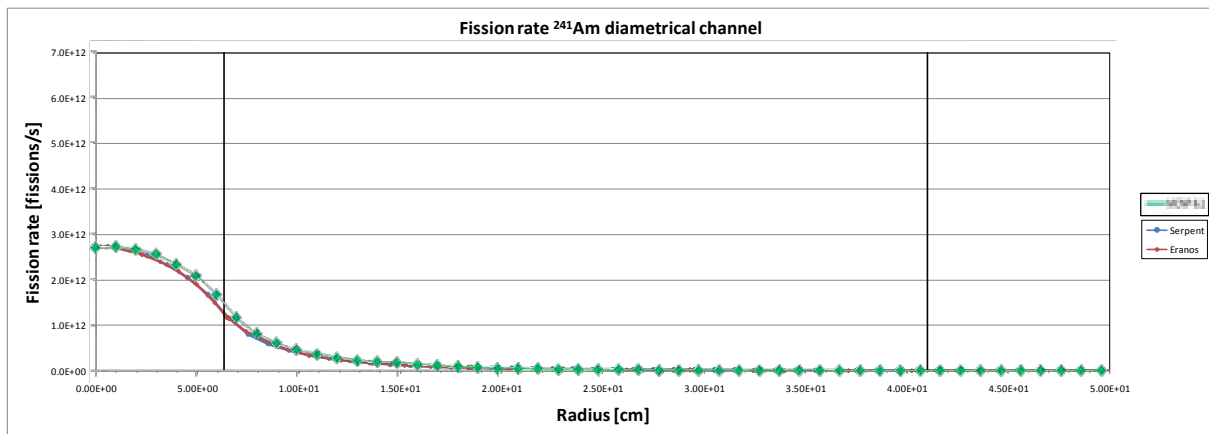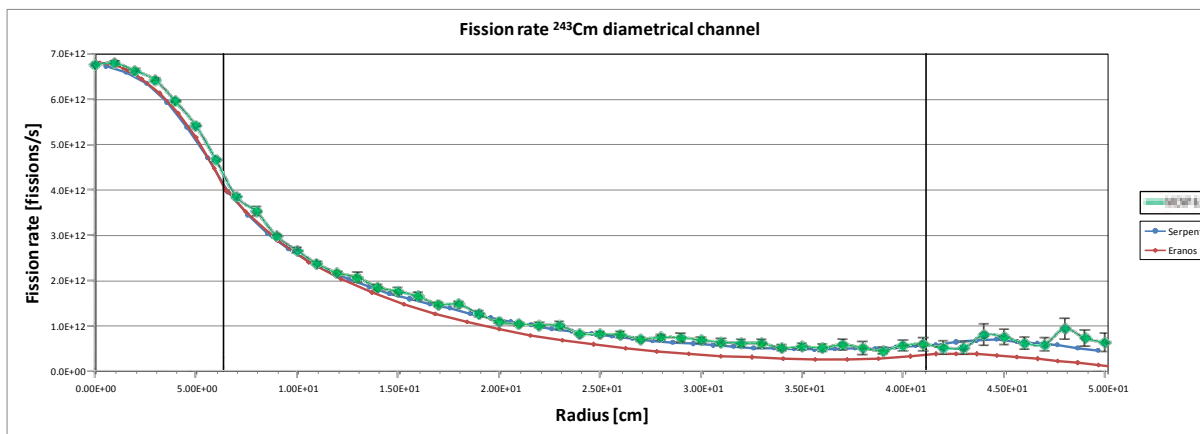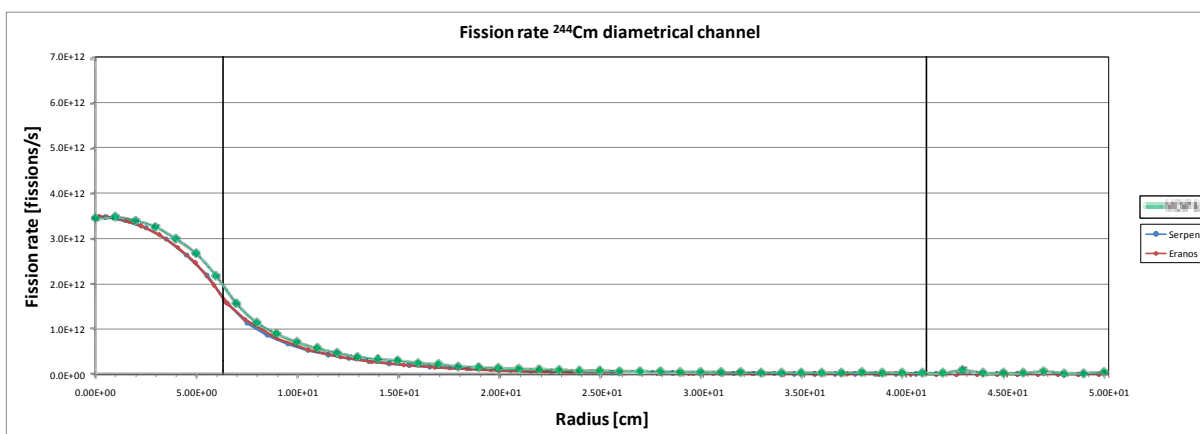

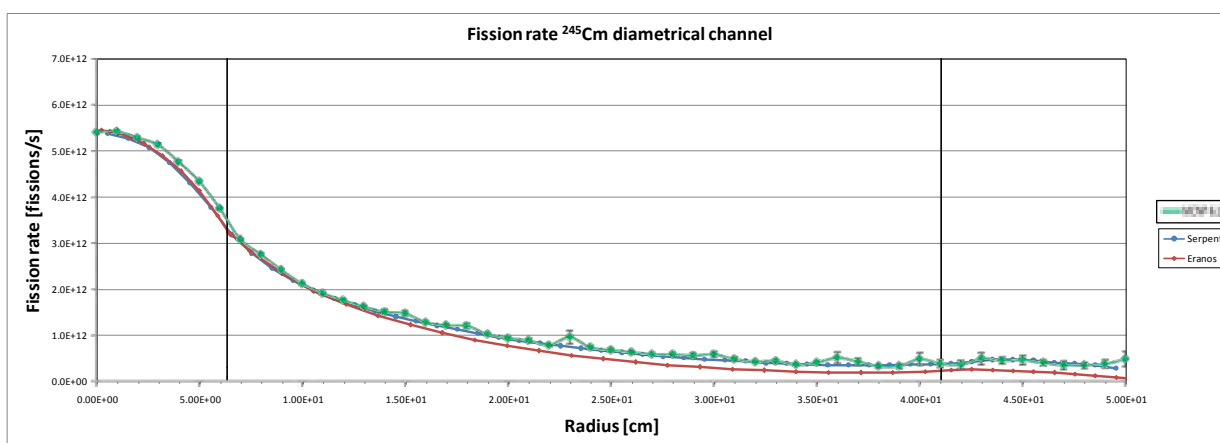**Figure 22 – [241]Am fission rate in the diametrical channel.**
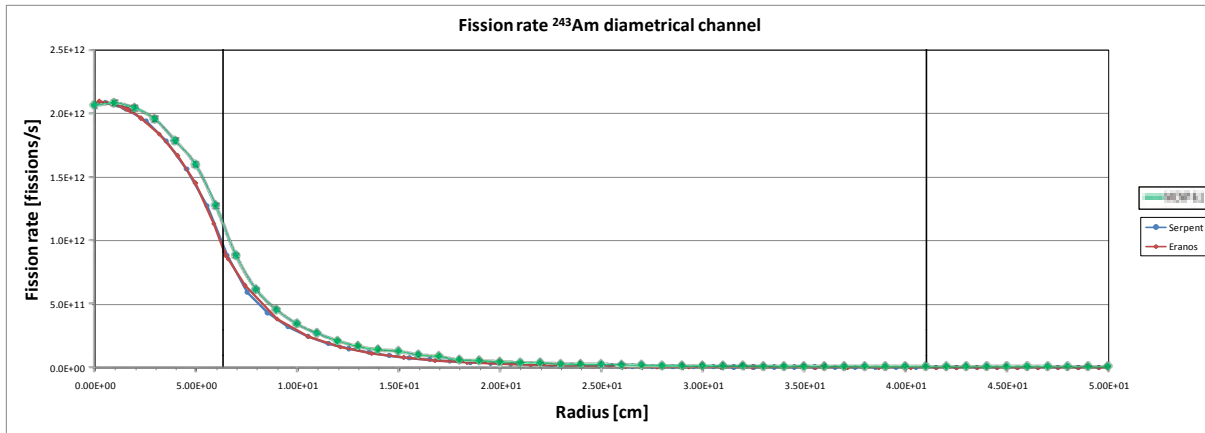
Figure 23 – ^{243}Am fission rate in the diametrical channel.
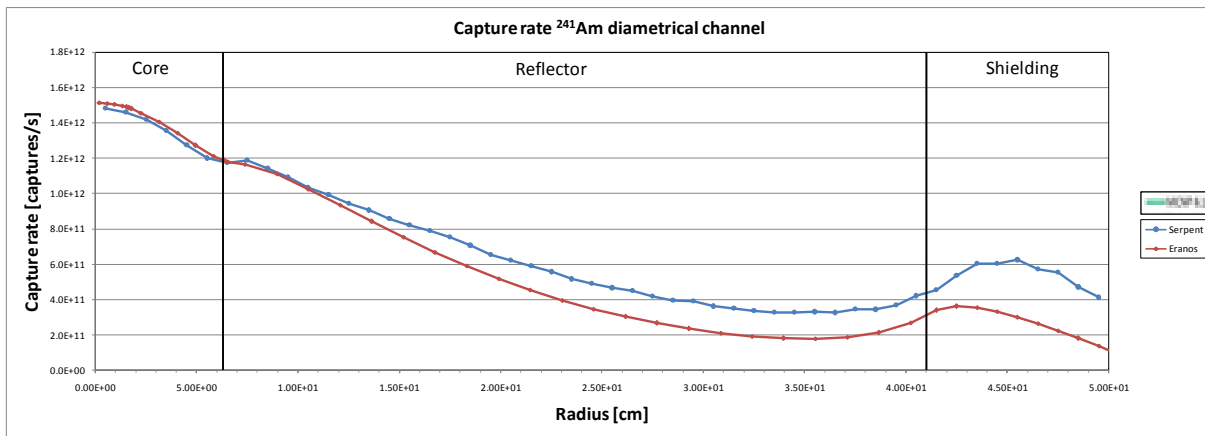
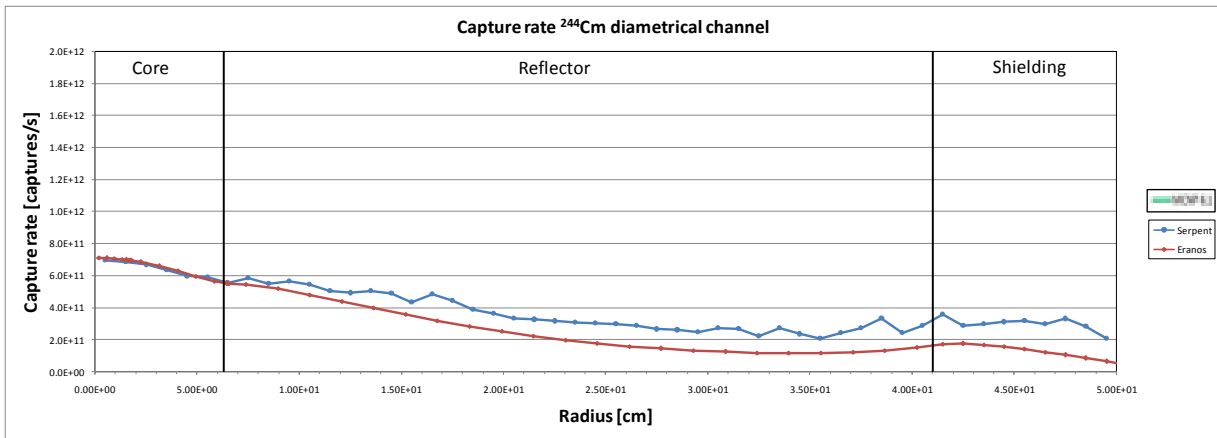**Figure 24 – ^{241}Am capture rate in the diametrical channel.**
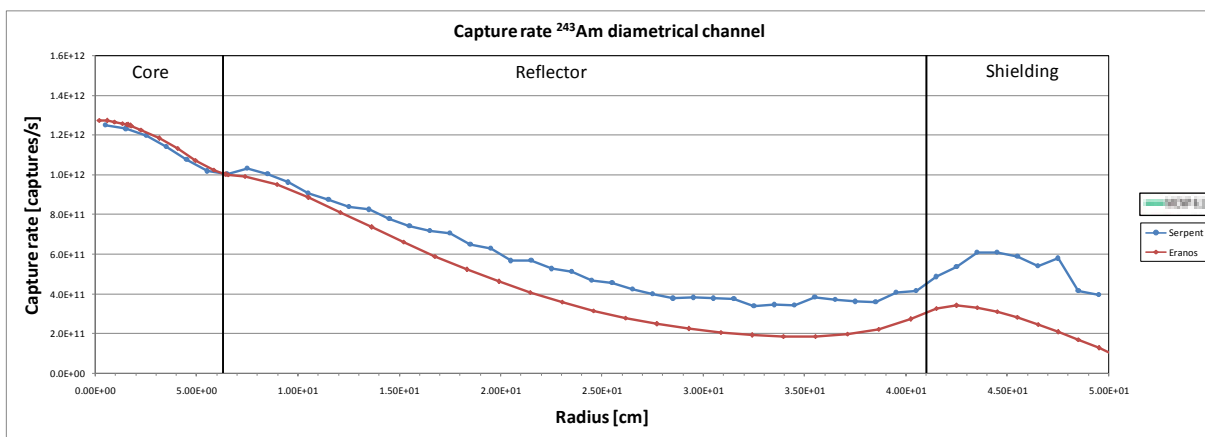
Figure 25 – ^{243}Am capture rate in the diametrical channel.

MCNP simulations for ^{241}Am and ^{243}Am fission reaction rates present an overestimation within the inner portion of the reflector as well as the reactor core. Errors are reported in the figure, even if small compared to plot scale.

Capture rates are about one order of magnitude lower from fission rates, and all results are compatible with the estimated flux traverse, the harmony between both code is better than in plutonium isotopes

rates. Relative errors for Serpent evaluation are between 0.07% and 5.5% for capture rate simulations and between 0.07% and 4% for fission rate simulations.

Figure 26 – ^{243}Cm fission rate in the diametrical channel.

Figure 27 – ^{244}Cm fission rate in the diametrical channel.

Figure 28 – ^{245}Cm fission rate in the diametrical channel.
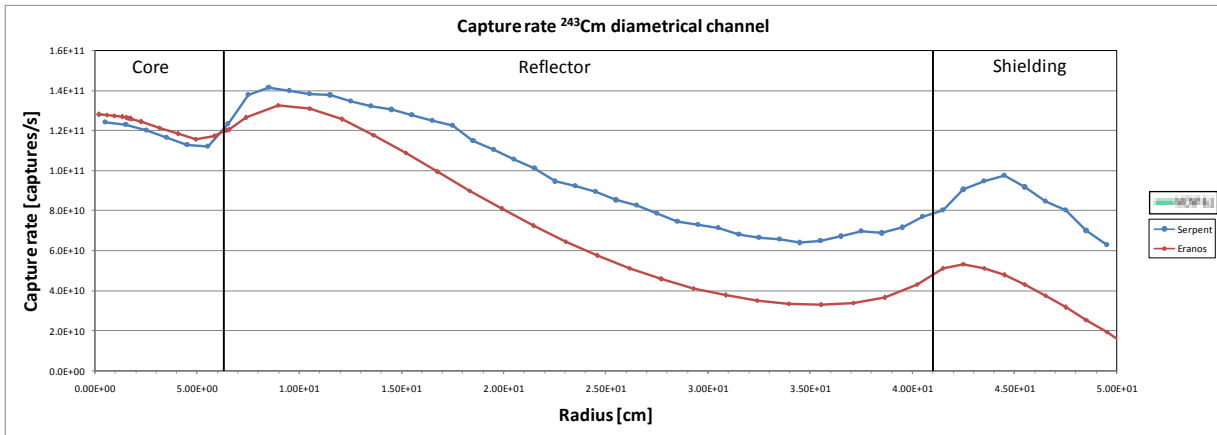
Figure 29 – ^{243}Cm capture rate in the diametrical channel.

Figure 30 – ^{244}Cm capture rate in the diametrical channel.
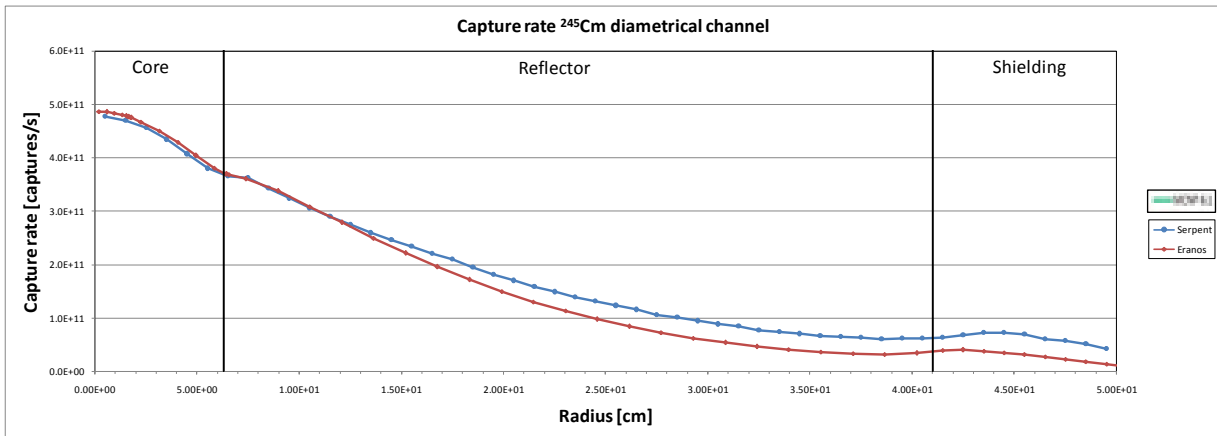
Figure 31 – ^{245}Cm capture rate in the diametrical channel.

Most common isotopes of curium in spent fuel are ^{243}Cm, ^{244}Cm and ^{245}Cm, respectively having half life of 29.1, 18.1 and 8500 years.

These elements show a regular decreasing trend for the fission rate (Figures 26-31) and a small peak in the first part of the shield.

Regarding ^{244}Cm, Serpent's databases doesn't contain data on total fission (MT = 18), and fission is given using the partial modes, so results showed are the sum of first and second-chance fissions (MT = 19 and 20). Fission rate obtained (Figure27) shows a typical even isotope behavior.

Moreover, MCNP simulations for ^{243}Cm, ^{244}Cm and ^{245}Cm fission reaction rates present aslight overestimation in the inner portion of the reflector as well as the reactor core – which is quite within calculation errors.

Capture rates (Figures from 29 to 31) showed different trends. If ^{243}Cm has its maximum at the end of the core, with another important peak at the end of reflector, with ^{244}Cm captures are more likely in core center.

Behavior of ^{245}Cm capture rate is similar to fission rate, but again with two small relative maximum.

Relative errors are between 0.05% and 2.5% in all cases, except for fission of ^{244}Cm. In fact errors related to MT = 20, due to lack of statistics, are elevated. Errors for total fission rate are calculated with the quadratic sum, because of the independence of functions leads to a null variance.Total fission rate errors are between 0.65% and 11%.

10.1   Average Microscopic Cross Sections

The possibility to extract flux and reaction rates traverses allow to have all the data to determine the average microscopic cross sections, relatives to the capture and fission of the selected minor actinides. The simple calculation has been performed using Microsoft Excel. The average microscopic cross sections have been calculated along the diametrical channel of TAPIRO and are defined as:

$$\bar{\sigma}(\vec{r}) = \frac{< \sigma(\vec{r}, E)\phi(\vec{r}, E) >_E}{< \phi(\vec{r}, E) >_E}$$

Where σ is the microscopic cross section and φ is the neutron flux. This parameter has been obtained as a ratio between the reaction rate and the flux for all meshes, along the diametrical channel. The average microscopic cross sections for all the selected minor actinides are shown in the following pages.

The MCNP simulation comparison is just preliminary since the relative errors need to be reduced and variance optimization possibly has to be implemented. Anyhow only fission reaction rates are presented in the present paragraph.
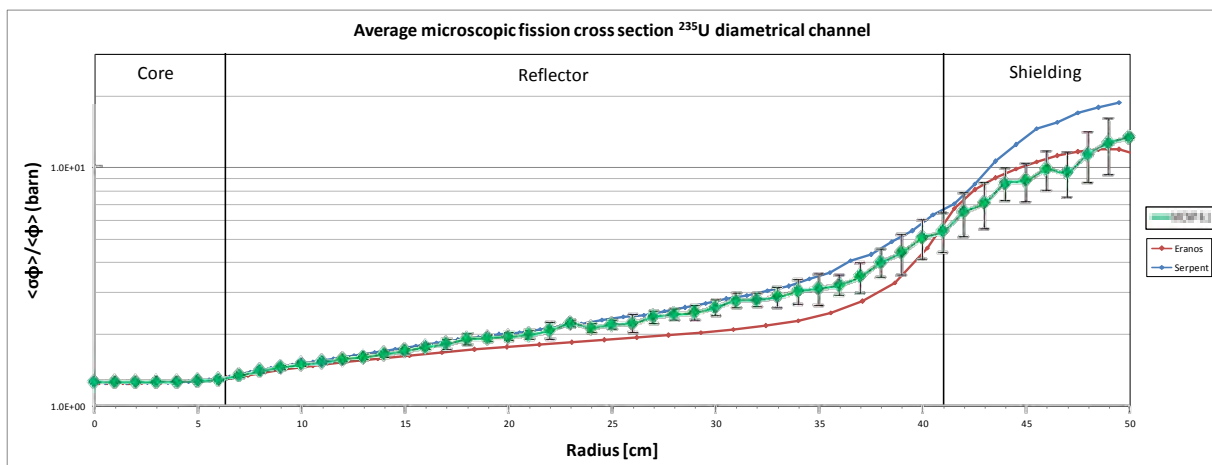

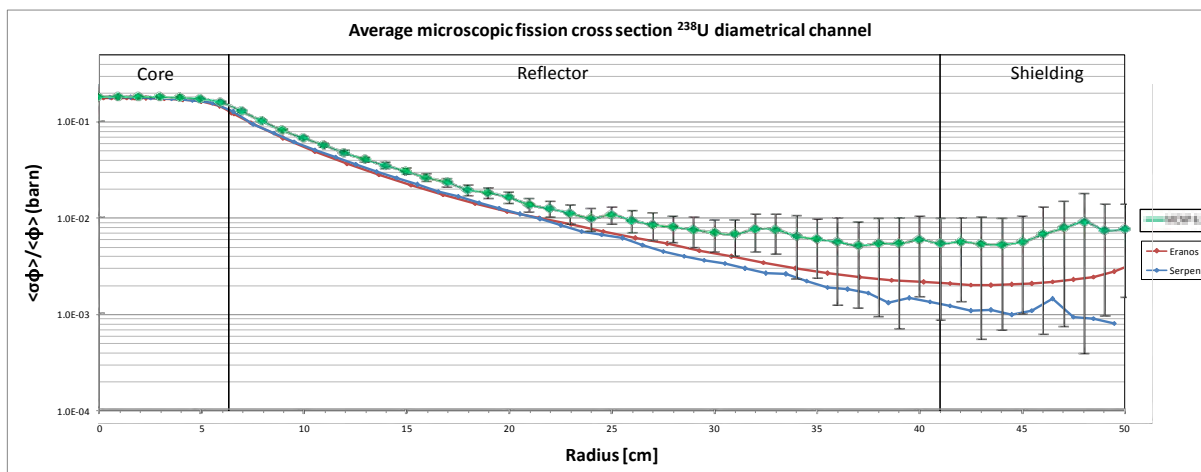**Figure 32 - ^{235}U average microscopic fission cross sections**

Figure 33 - ^{238}U average microscopic fission cross sections

As we can see in Figure 32 , values of ^{235}U fission cross section have a monotonic increase, passing from fast to epithermal and thermal spectrum, as expecting from a fertile material reaching about 20 b in the points far from core center, while ^{238}U fission cross section (Figure Figure 33), like expected from a fertile material, is higher and about constant into the core, where neutrons are fast, and rapidly decrease where neutrons become epithermal and thermal, passing from 0.2 to 0.001 b.
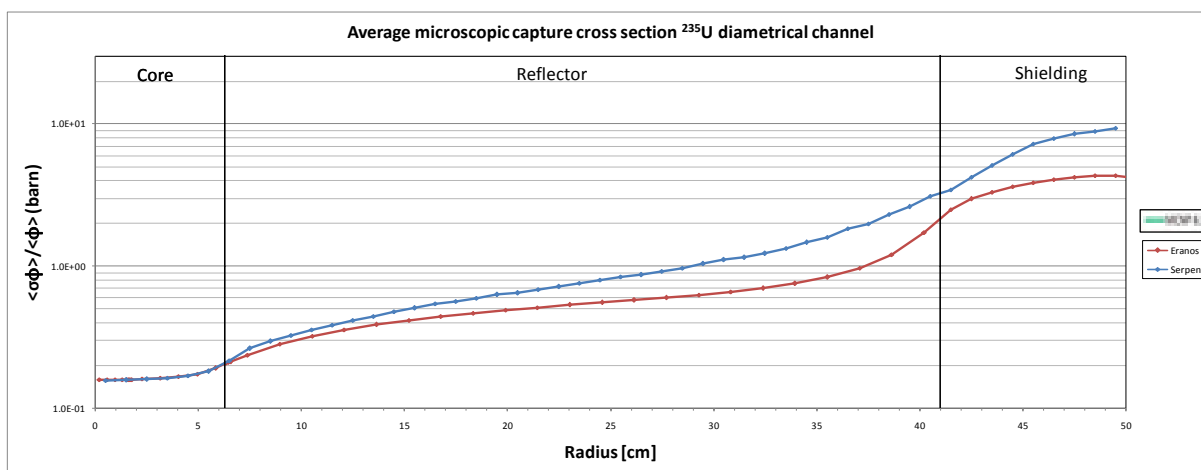
Figure 34 - ^{235}U average microscopic capture cross sections
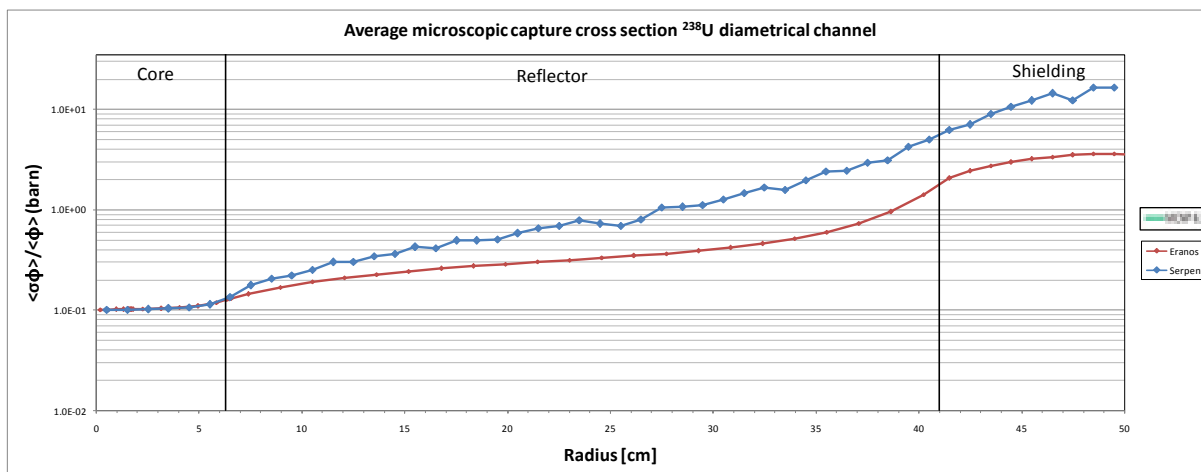
Figure 35 - ^{238}U average microscopic capture cross sections

Regarding capture cross section, Figures 34 and Figure 35 showed a behavior increasing starting from center, revealing that captures are more likely with slow neutrons. Changes of inclination correspond to relative maximum of reaction rates.

Relatives errors are between 0.007% and 2% for ^{235}U cross sections, and between 0.07% and 20% for ^{238}U cross sections.
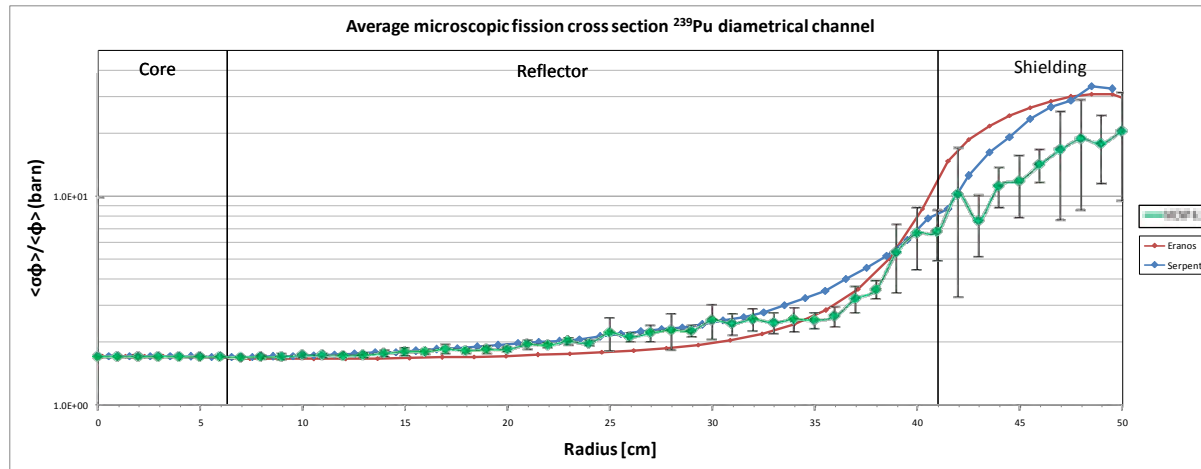
Figure 36 – ^{239}Pu average microscopic fission cross sections
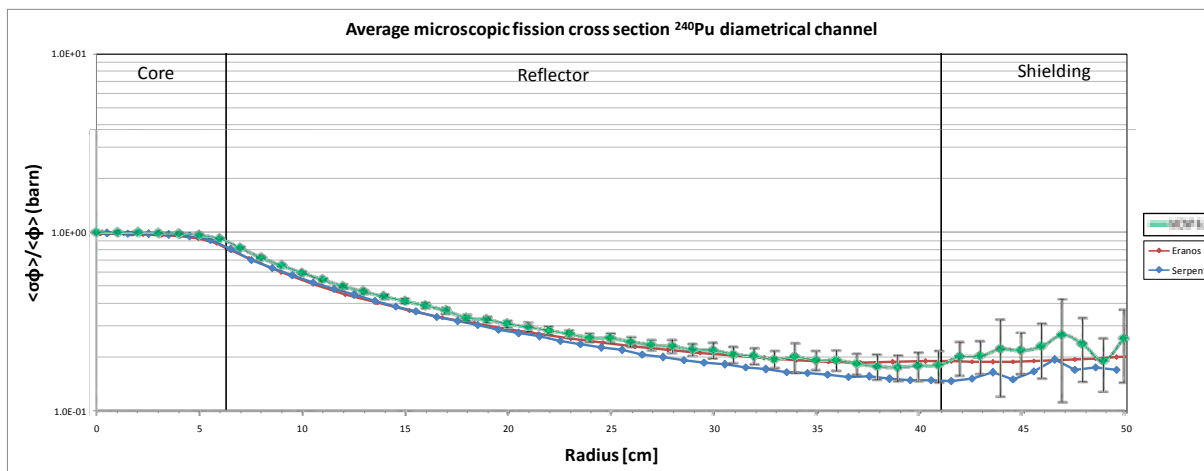
Figure 37 – ^{240}Pu average microscopic fission cross sections
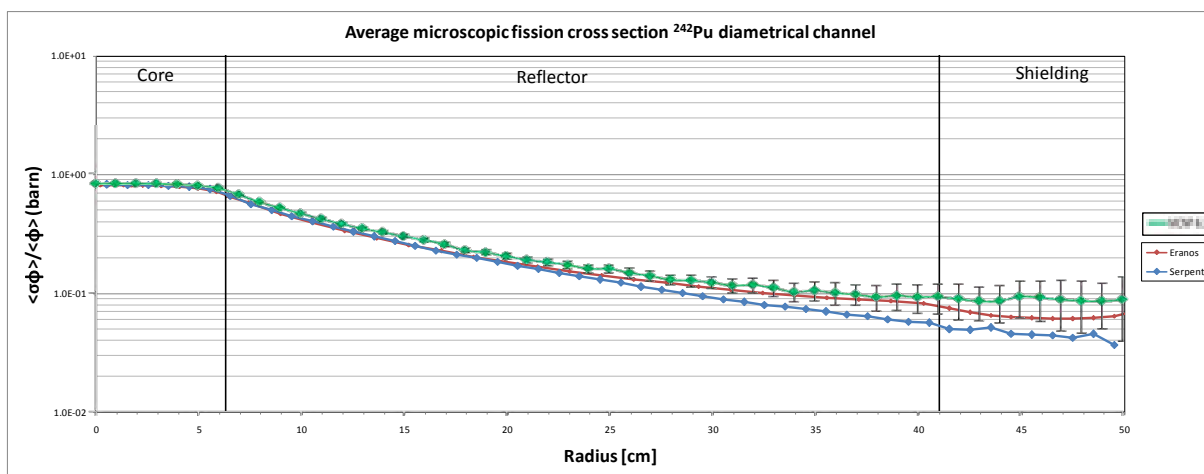
Figure 38 – ^{242}Pu average microscopic fission cross sections

The differences emerged for uranium fission are still present for plutonium fission (Figures 36-38). The average microscopic fission cross sections are more close in the core and then they follow a very different trend: ^{239}Pu increases moving to the shield while the others decrease. In fact the odd isotopes of plutonium is fissile while the other two are fertile.
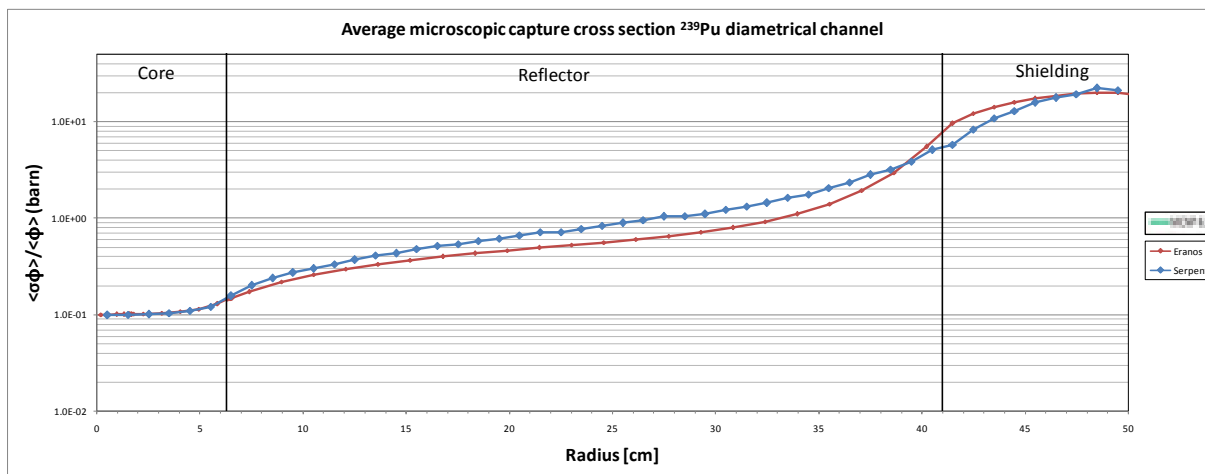
Figure 39 – ²³⁹Pu average microscopic capture cross sections
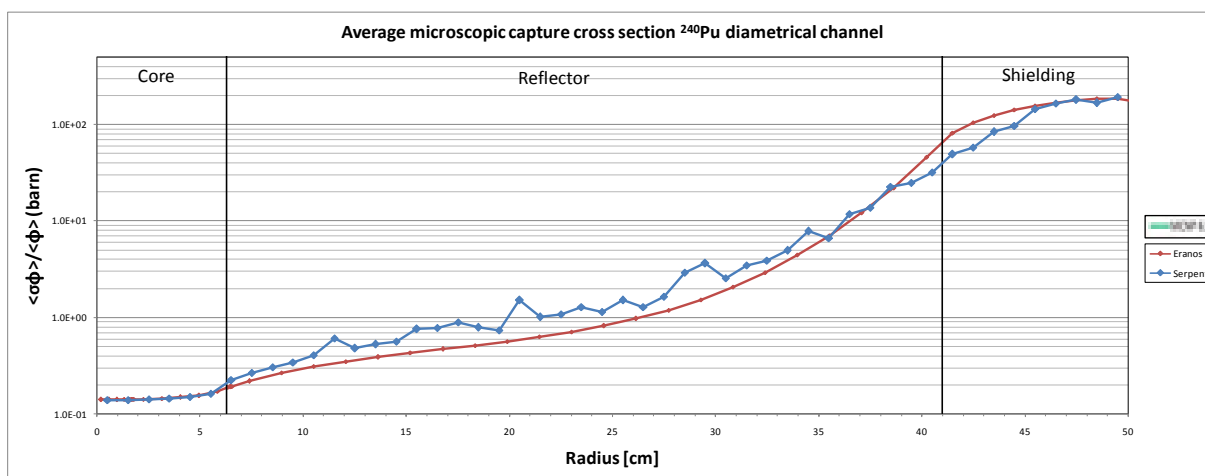
Figure 40 – ²⁴⁰Pu average microscopic capture cross sections
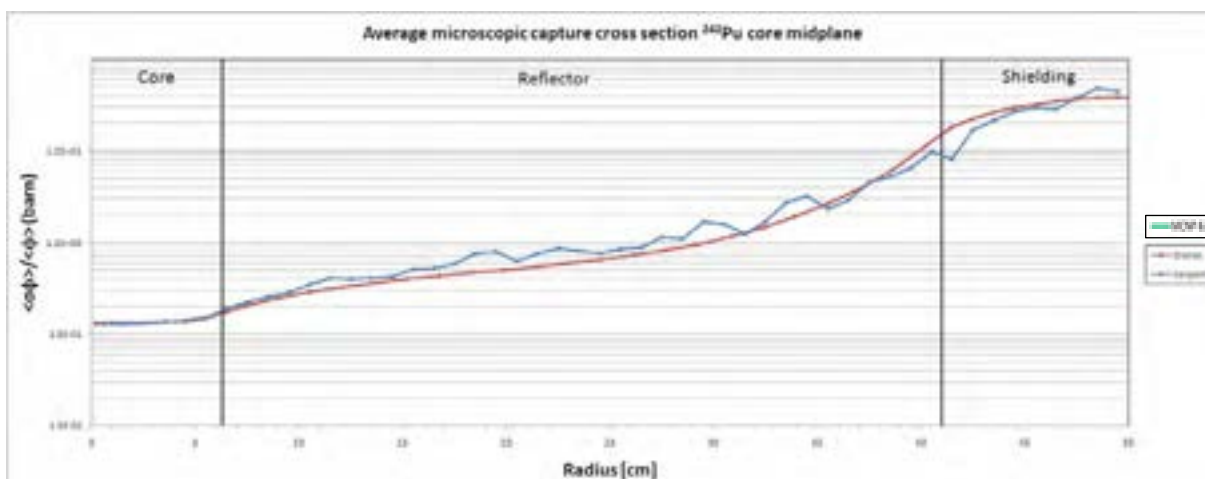
Figure 41 – ²⁴²Pu average microscopic capture cross sections

In the case of ^{240}Pu this is even the absolute maximum, revealing that capture are more probably with slow neutrons (Figure 40). The highest values are again far from core, due to reduction of neutron population and consequently reduction of statistics.

For the capture reaction (Figures 39-41) there is a global increasing trend for all the nuclides. The values are very close till the first part of the reflector than they are a little bit different but maintain the same proceeding.

Relative errors are between 0.05% and 4% for Fission cross sections, while are between 0.06% and 15% for capture cross sections.
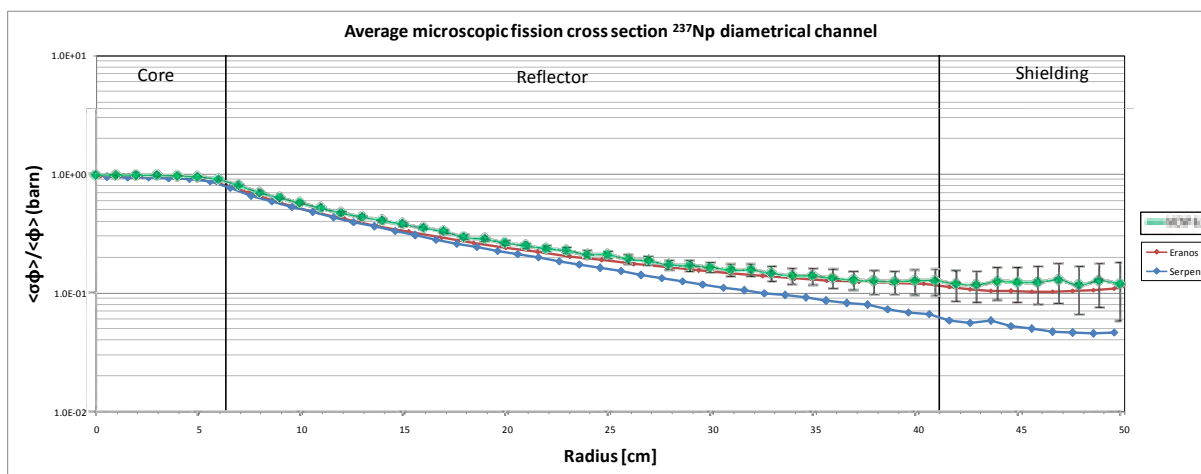
Figure 42 - ^{237}Np average microscopic fission cross section
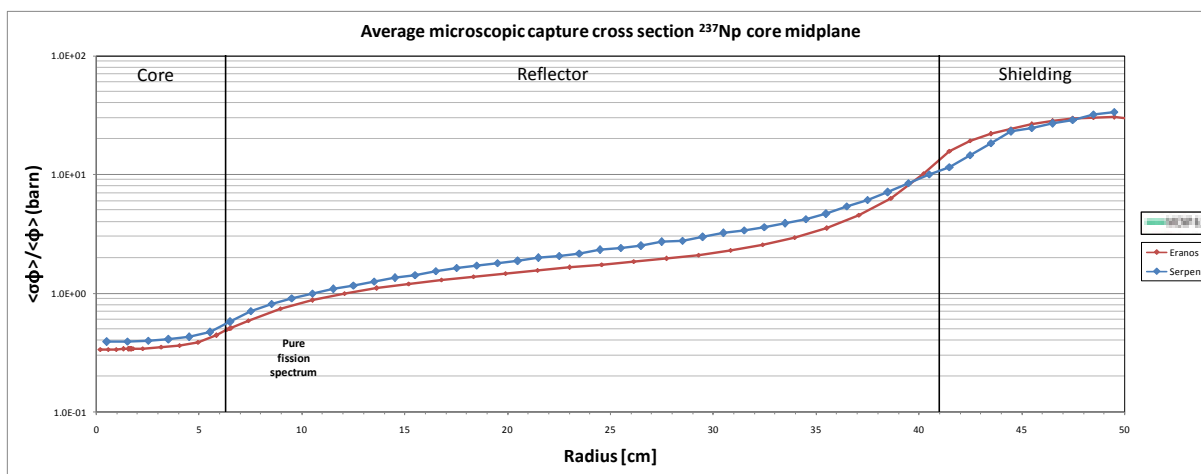
Figure 43 - ^{237}Np average microscopic capture cross section

As pointed out in Fission rate, ^{237}Np is fissionable by fast neutrons, and Figure 42 shows as fission cross section is more elevated into the core, where has the value of 10 b, and rapidly decreases along the channel. Capture cross section of ^{237}Np increase along the channel, until reaching value of 30 b in the points far from core center (Figure 43).

Relative errors associated to Serpent simulations are between 0.03% and 4%.

Both ^{241}Am and ^{243}Am fission cross section (Figures 44-45)initially have a decrease from core center, but also an ascent at the end of the reflector, more relevant in ^{241}Am behavior.
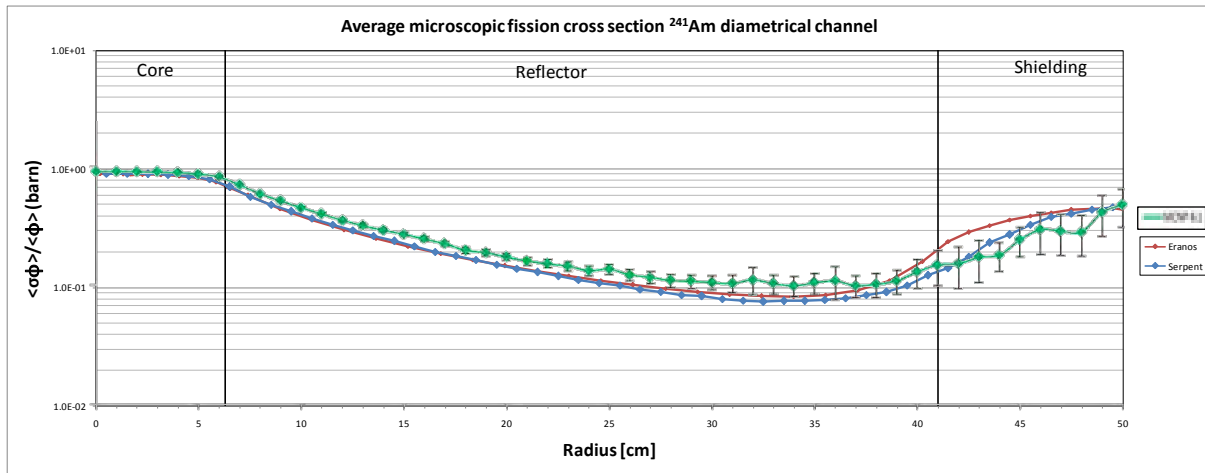
Figure 44 – ²⁴¹Am average microscopic fission cross section
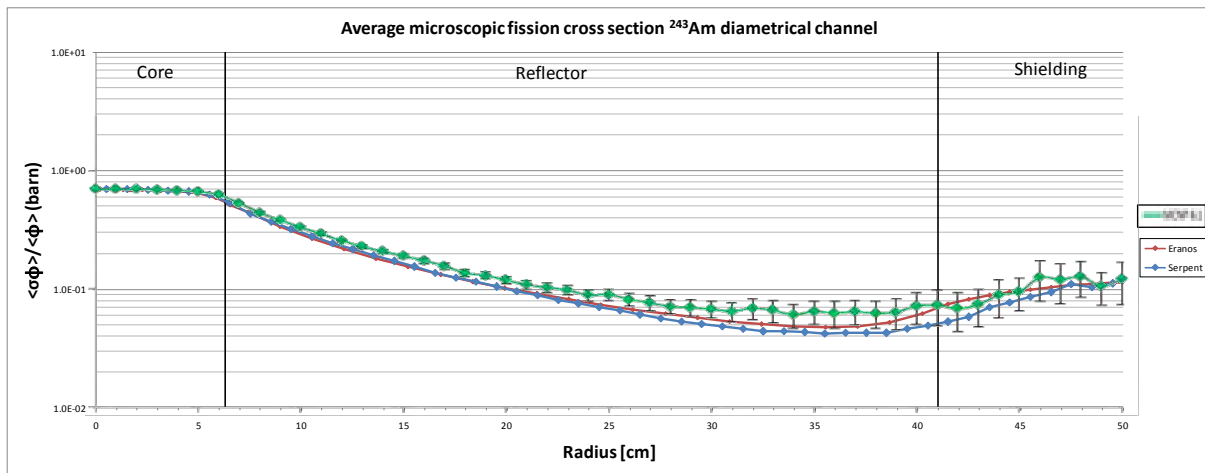

Figure 45 – ²⁴³Am average microscopic fission cross section

The americium average fission cross section (Figures 44-45) has the same trend for both isotopes; the cross section decrease outside the core than start to increase again just before the shield but it remains lower than the core values.
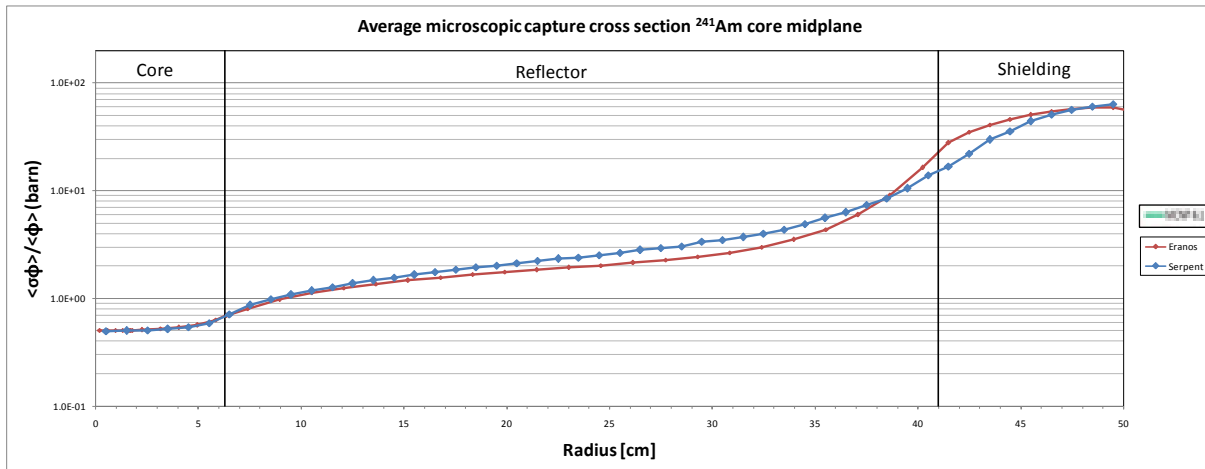

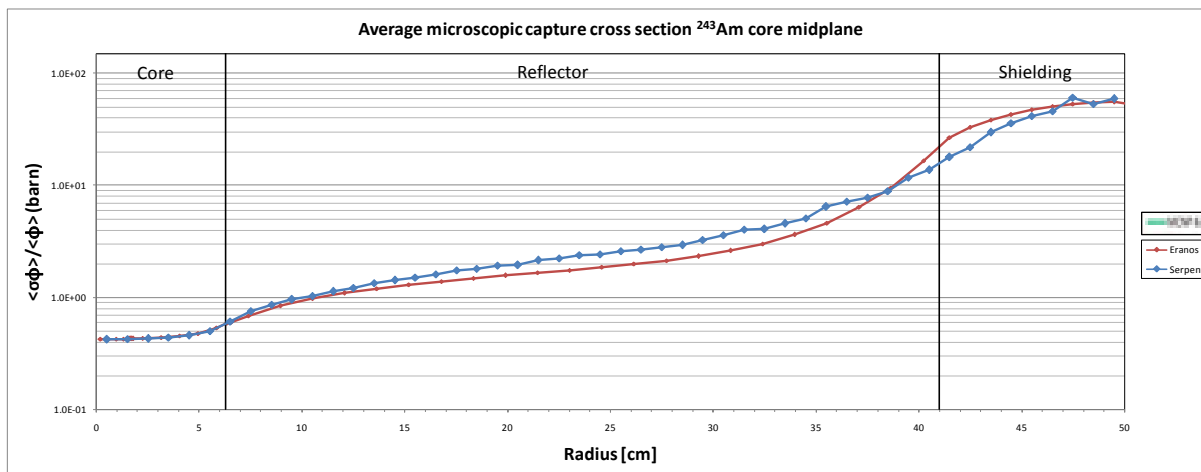**Figure 46 – ²⁴¹Am average microscopic capture cross section**

Figure 47 – ^{243}Am average microscopic capture cross section

The regularity is maintained also in the capture (Figures 46-47); in this case there is an increasing trend and for the two isotopes there is almost a perfect coincidence of the curves above all in the external part of the system.

Relative errors are between 0.05% and 4% for fission cross sections and between 0.05% and 6% for capture cross sections.

Behavior of ^{243}Cm and ^{245}Cm are similar and monotonic increasing, reaching respectively values of 70 and 50 b in the last point of the channel, where there is a soft spectrum.

Regarding ^{244}Cm, values are again sum of two cross section, regarding first and second-chance fission, as Serpent databases don't have information about total fission of this isotopes. The behavior obtained is similar to the one of americium isotopes, with an ascent at the terminal part of the channel.
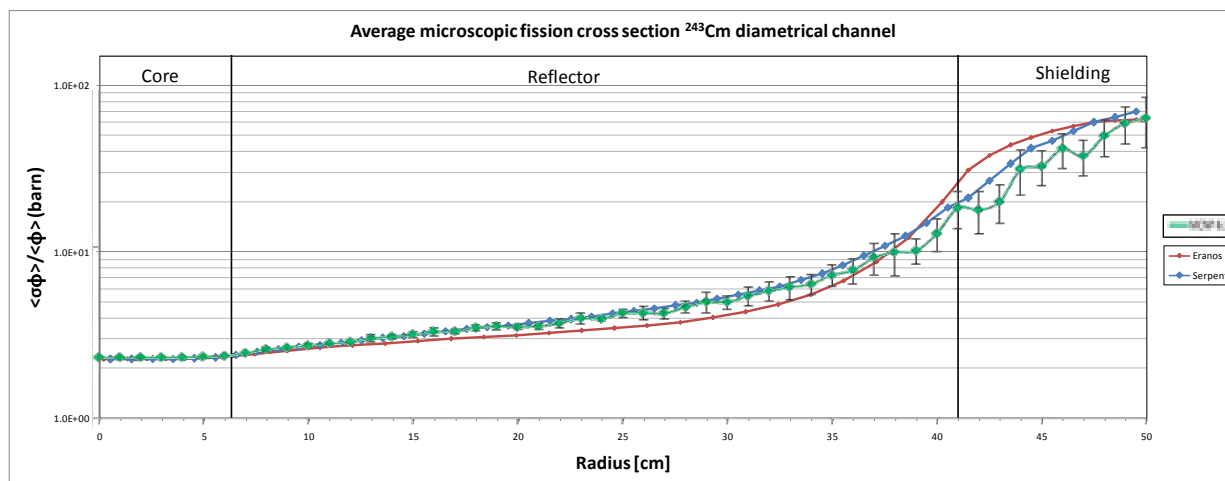

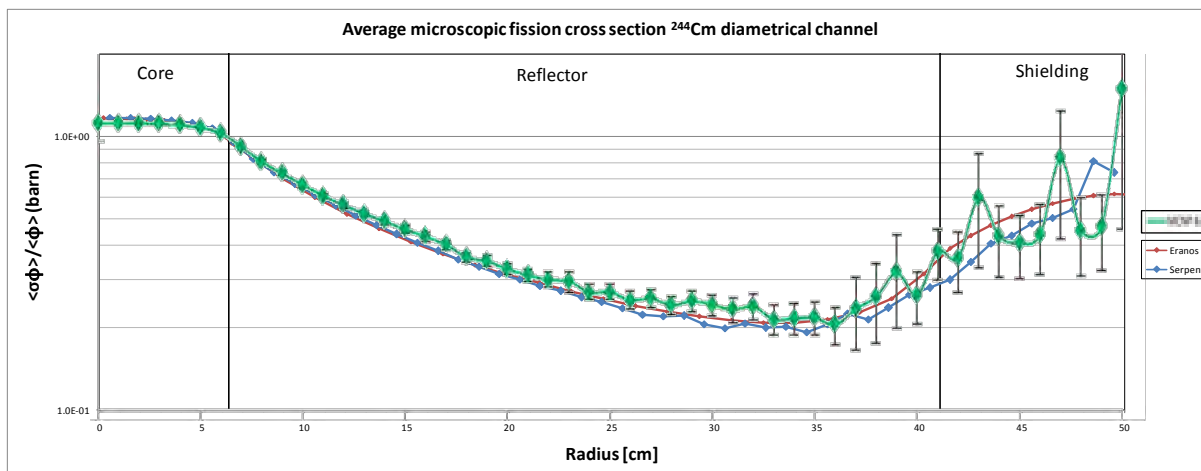**Figure 48 – ^{243}Cm average microscopic fission cross section**

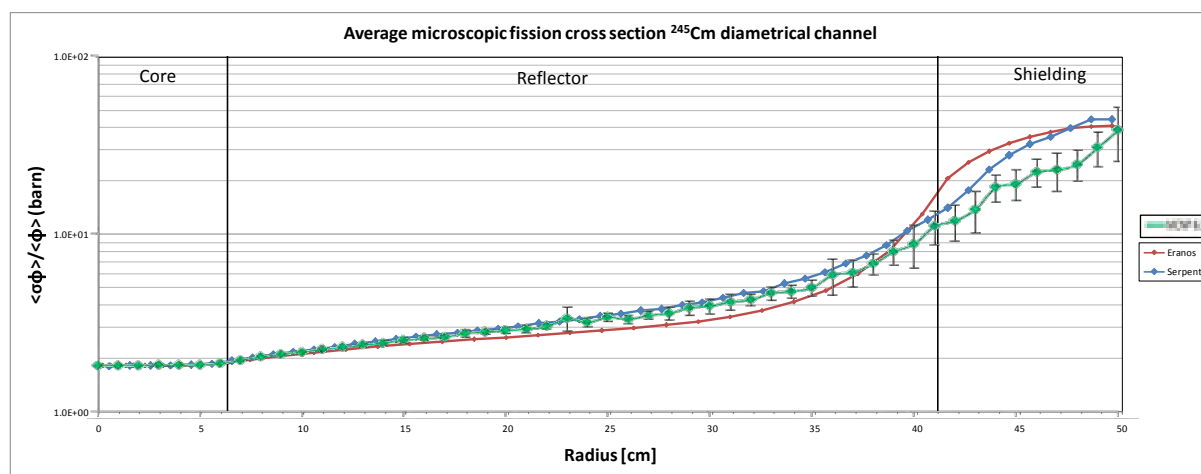**Figure 49 – ^{244}Cm average microscopic fission cross section**

Figure 50 – ^{245}Cm average microscopic fission cross section

^{243}Cm and ^{245}Cm have the same shape of the average fission cross sections (Figures 48-50). ^{244}Cm decreases outside the core, differently from the others.

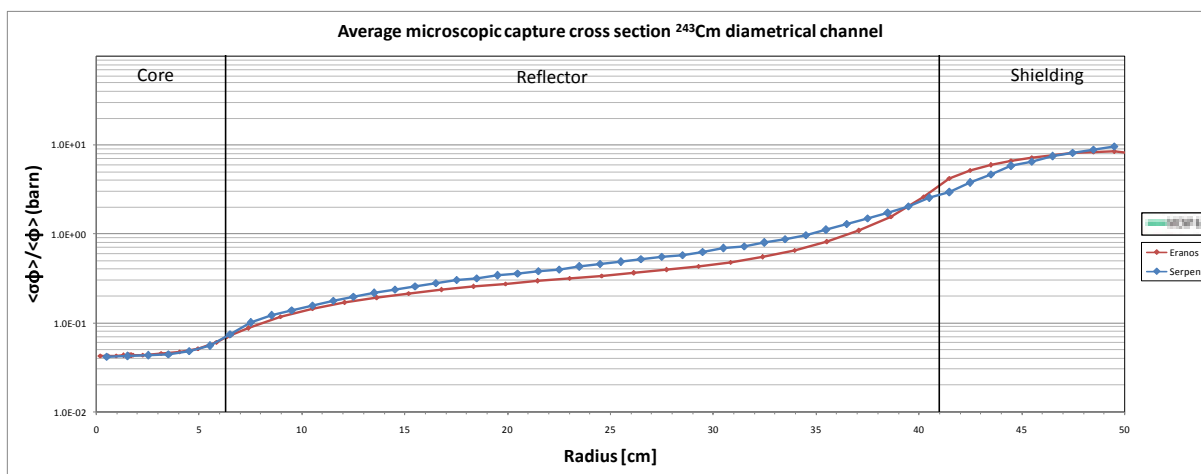**Figure 51 – ^{243}Cm average microscopic capture cross section**
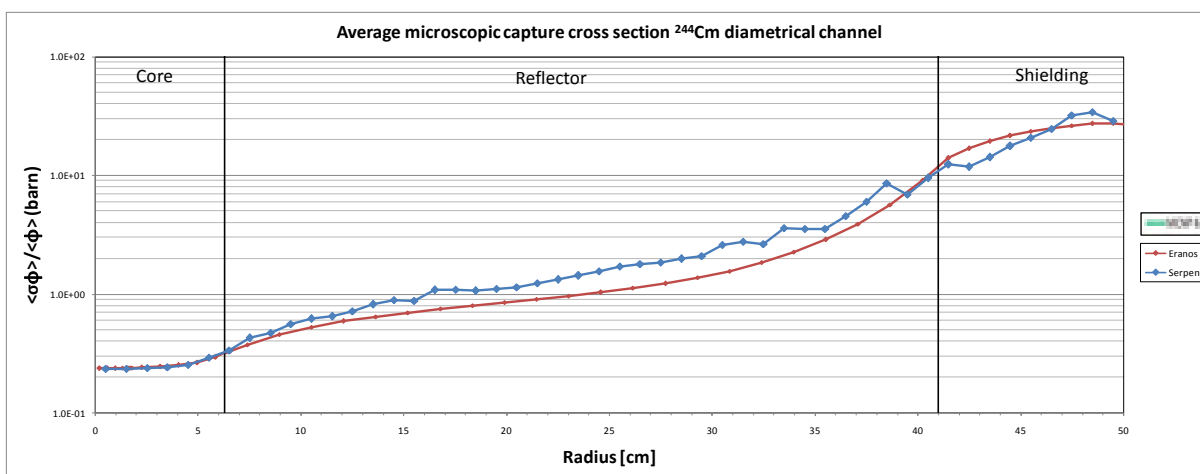
Figure 52 – ²⁴⁴Cm average microscopic capture cross section
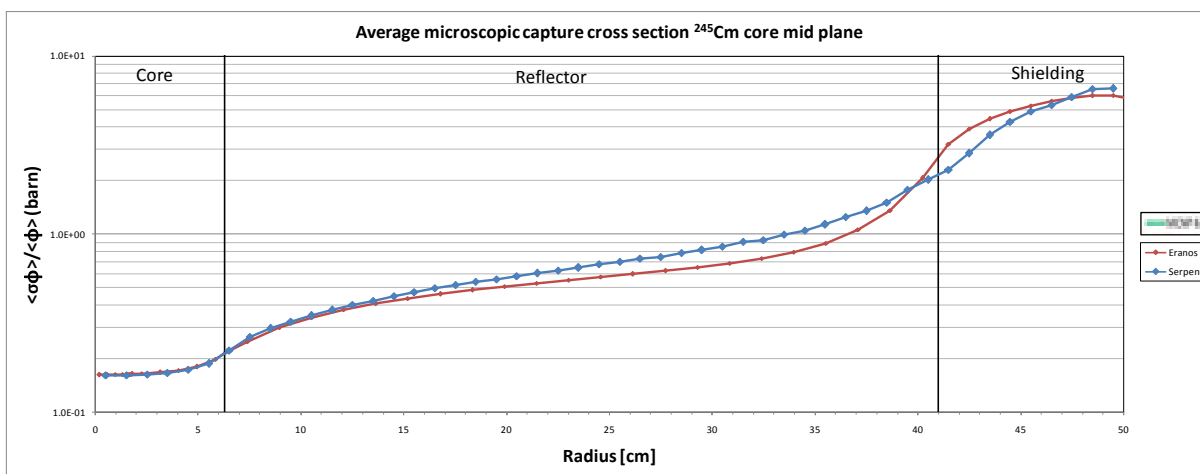

Figure 53 – ²⁴⁵Cm average microscopic capture cross section

All the curium isotopes show a similar increasing trend for the capture (Figures 51-53).

Relative Serpent errors are between 0.04% and 2.5% for ^{243}Cm and ^{245}Cm, for both fission and capture cross sections, while for ^{244}Cm are between 0.06% and 15%.

7.2 Capture to Fission Ratio

Combining the average microscopic capture and fission cross section is possible to determine the capture-fission ratio (α) for all the nuclides. This parameter has a key role in the irradiation of minor actinides. The advantages obtained irradiating minor actinides with a fast spectrum depend on this parameter. Capture-fission ratios for isotopes analyzed are shown in further figures.

Since it changes considerably with energy, showing how in a fast neutron spectrum, there is more competition between capture and fission respect to a thermal neutron spectrum.

Relative errors for Serpent results have been calculated following formulation of errors propagation.
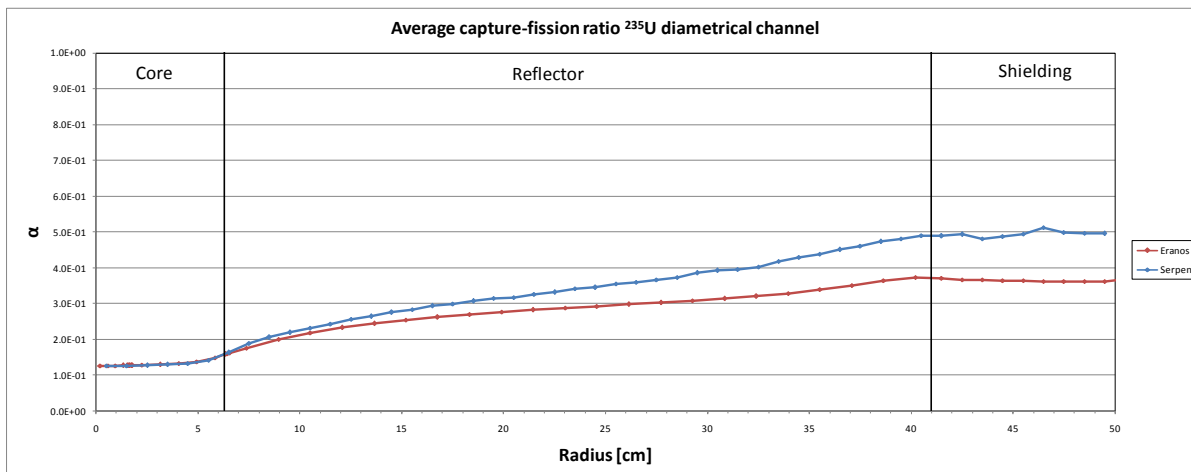
Figure 54 - ^{235}U capture-fission ratio

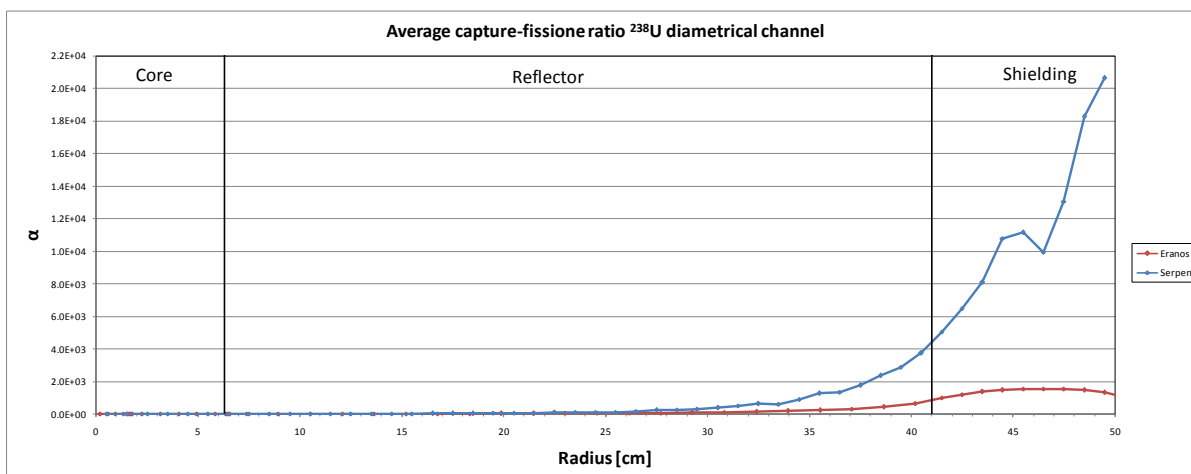
Figure 55 - ^{238}U capture-fission ratio

Figure 54and Figure 55showed how α is growing from core center to the shielding. But, if for ^{235}U the change is of few tenths, with constant values in the core and in the shield, for ^{238}U the growth never stopped, and is four order of magnitude higher. Relative errors for Serpent code are between 0.04% and 3% for ^{235}U and between 0.08% and 20% for ^{238}U.
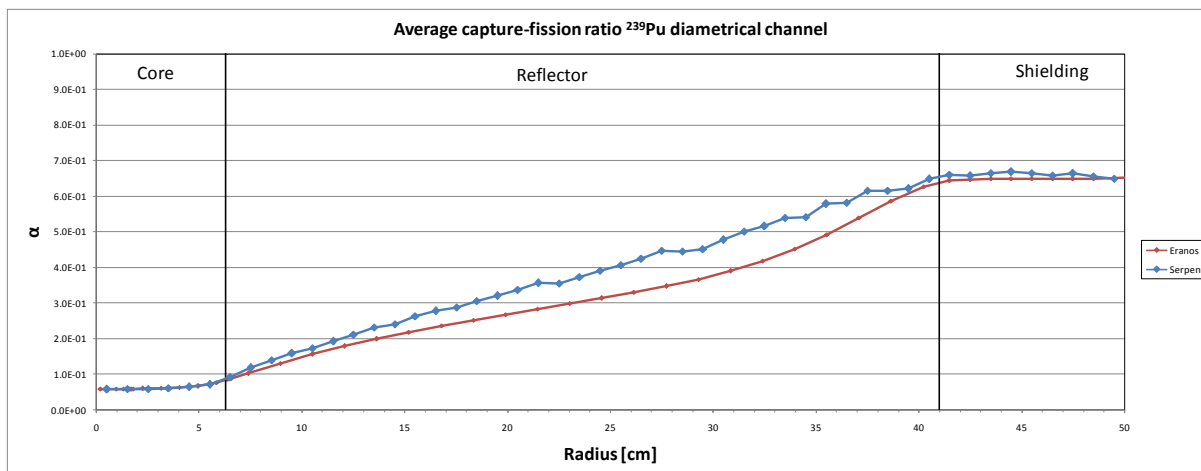
Figure 56 - ^{239}Pu capture-fission ratio

Figure 56shows like, again, the odd isotope of plutonium has a behavior similar to ^{235}U, with increasing values in the reflector and two plateau into the core and into the concrete shield.Values are a little bit different but they have the same order of magnitude of ^{235}U.
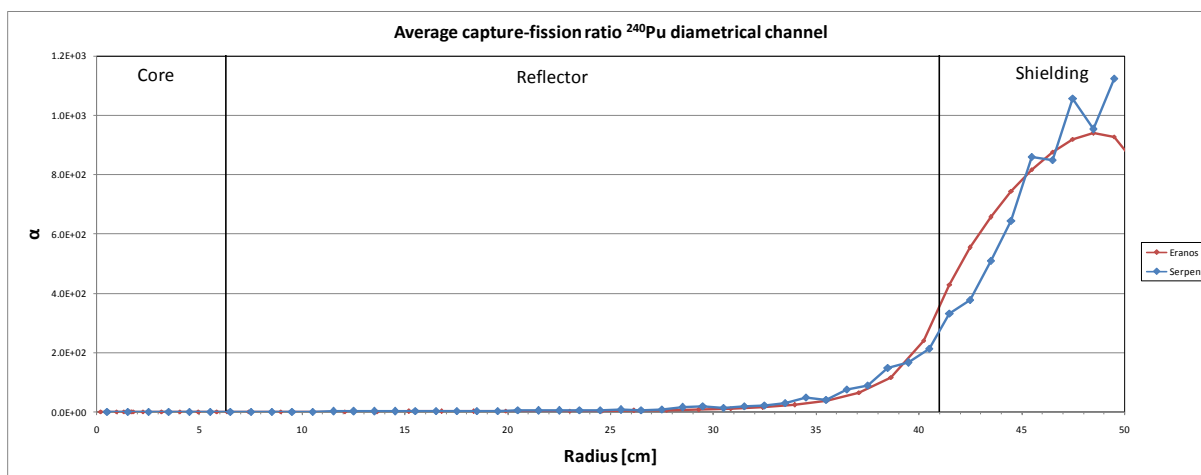

Figure 57 - ^{240}Pu capture-fission ratio
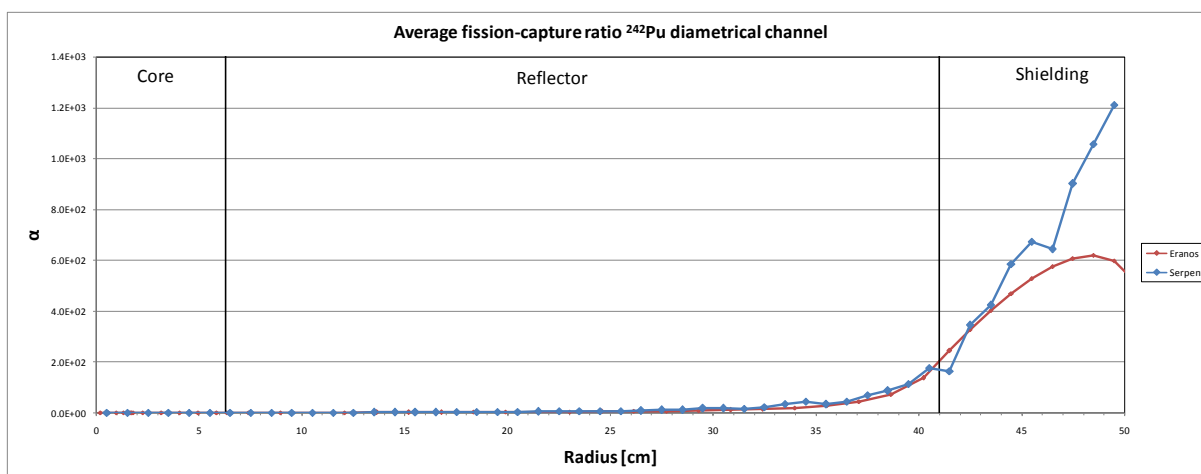
Figure 58 - ^{242}Pu capture-fission ratio

Conversely, ^{240}Pu and ^{242}Pu (Figure 57, Figure 58) have the typical behavior of even isotopes, with exponential growth and changes of many order of magnitude between fast and thermal neutron spectrum.

Relative errors are between 0.05% and 5% for ^{239}Pu, between 0.05% and 20% for ^{240}Pu and between 0.06% and 15% for ^{242}Pu.
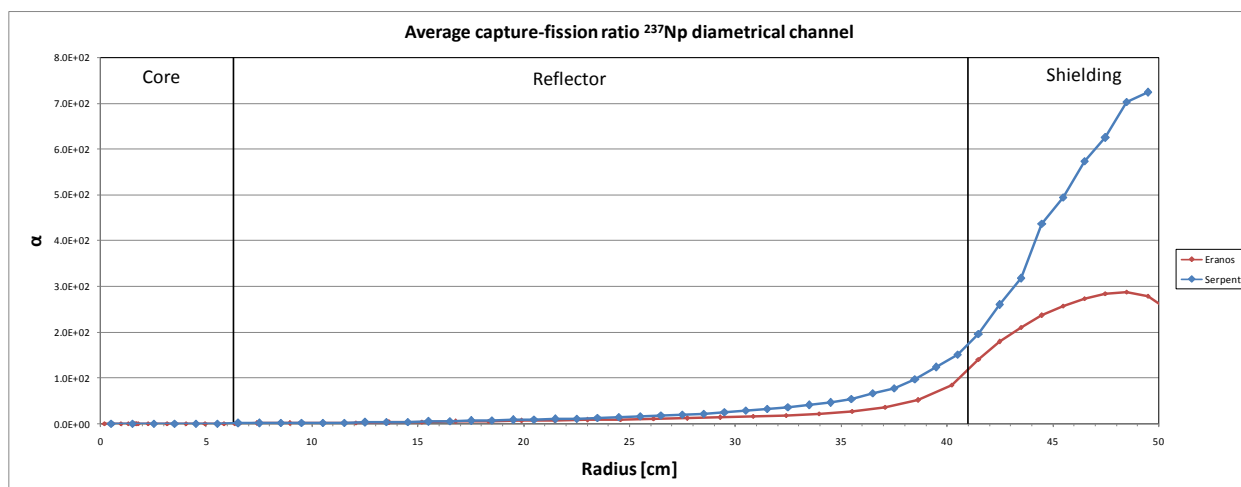
Figure 59 - ^{237}Np capture-fission ratio

As noticed for plutonium and uranium isotopes, a very similar trend characterizes neptunium (Figure 59). The neptunium α is over 500 at the end of diametral channel for Serpent evaluation; relative errors in this case are between 0.06% and 5.5%.
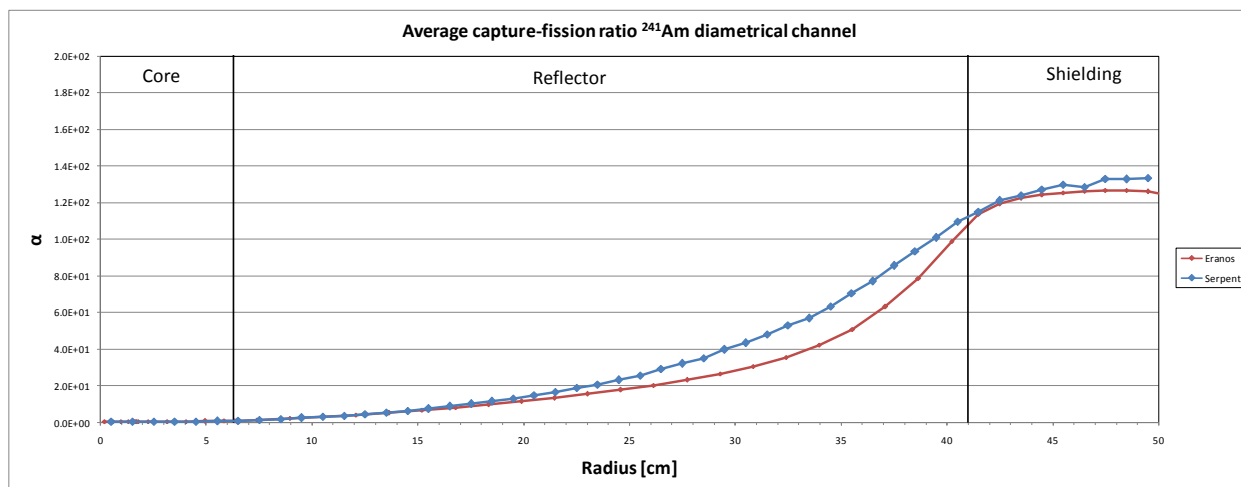
Figure 60 - ^{241}Am capture-fission ratio

Figure 60 shows the typical trend described for the isotopes of uranium and plutonium.
The difference is that in the case of ^{241}Am the curve starts to increase earlier. This feature characterizes also ^{243}Am (Figure 61) but less than ^{241}Am.
Relatives Serpent statistical errors are between 0.07% and 6.5% for both isotopes.
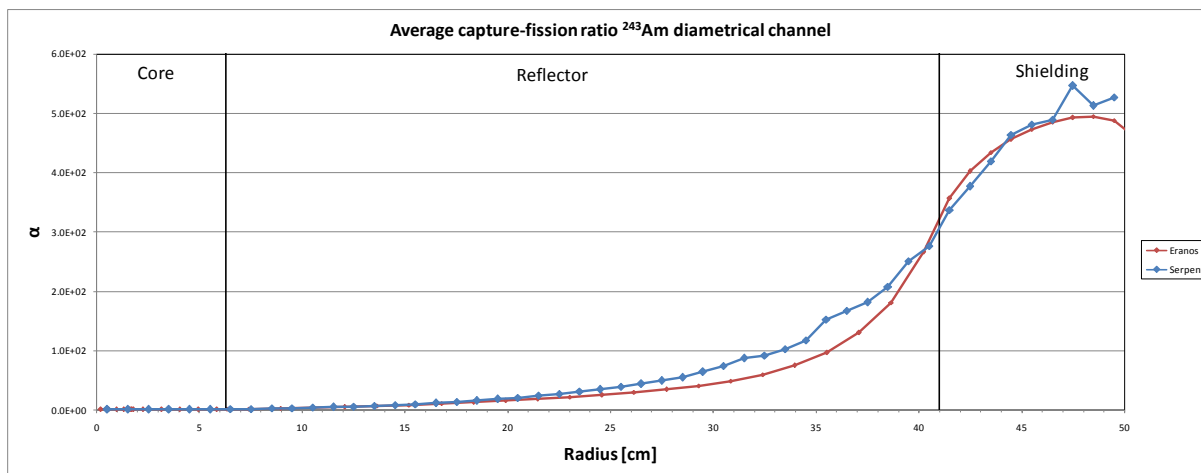
Figure 61 - ^{243}Am capture-fission ratio
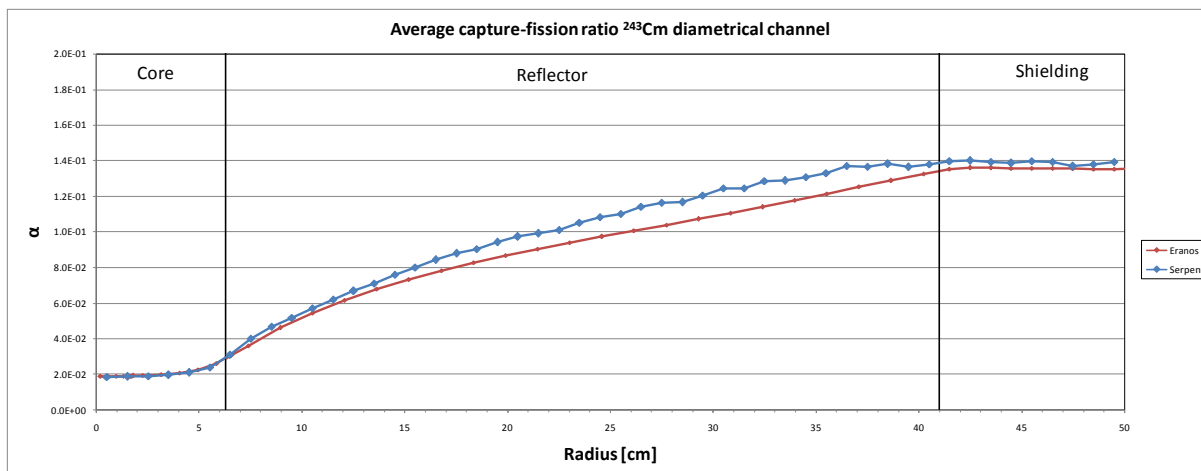
Figure 62 - ^{243}Cm capture-fission ratio

Differently from the other minor actinides, ^{243}Cm (Figure 62) presents a trend similar to the ^{235}U one (Figure 54). In the case of ^{243}Cm, contrarily to uranium, the higher value is not reached inside the reflector. Otherwise, ^{244}Cm (Figure 63) shows a trend analogous to americium isotopes (Figure 6361).

Figure 63 - ^{244}Cm capture-fission ratio

Figure 64 - ^{245}Cm capture-fission ratio

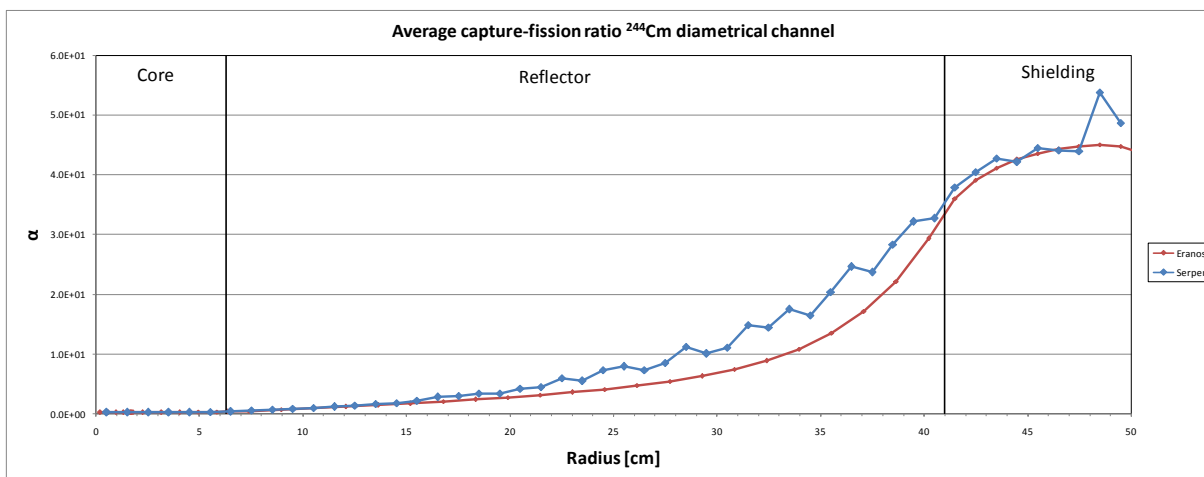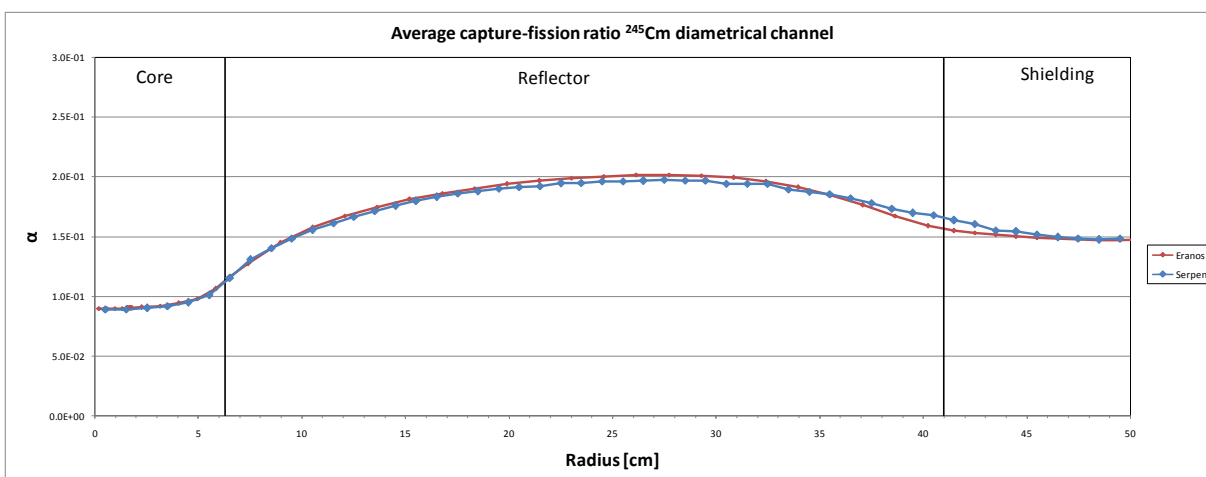Figure 64 is different from all others isotopes. The main characteristic of the ^{245}Cm is that the maximum value of α is reached approximately in the middle of the reflector and then the curve start to decrease maintaining a final value bigger than the initial one.

For this isotope differences between minimum and maximum are of few tenth.

Relative errors are between 0.06% and 4.5% for ^{243}Cm and ^{245}Cm, while for ^{244}Cm, for which cross section errors are already calculated with errors propagation, are between 0.06% and 19%.

Obviously, all these trends are a direct consequence of the different fission and capture cross sections of the selected nuclides. The importance of these graphics lies in the fact that they can be very useful to analyze the behavior of the selected nuclide in relations to capture and fission reactions, and for different positions inside the diametrical channel of the system.

11. Activation results.

The aim of these calculations is to evaluate the possibility to fulfill activation measurements in TAPIRO, in order to access capture cross sections of minor actinides, analyzing the (n,γ) activation chains [16]. The feasibility of this experience depends on different factors such as the activity level of the samples after irradiation (that influence the cooling time after which would be possible extract the samples from the system without radiological risks for the operators) and the energy of the γ-rays emitted. This last information is fundamental for the counting rate estimation and it influences the necessary detector type. The features of the neutron spectrum used for these activation calculations have been determined through the ERANOS/Serpent calculations described previously, for three different positions inside the diametrical channel: equivalent to tangential channel, centre reflector and centre shield. For these preliminary analysis six OSMOSE (Oscillation in MINERVE of isotope in 'Eupraxic' Spectra)[4] samples have been chosen, according to the CEA. The samples contain ^{237}Np,

---

[4] This program is finalized to measure the integral absorption rates of minor actinides using the oscillation technique in MINERVE, a CEA research reactor sited in Cadarache. The program is a DOE-CEA collaboration.

[242]Pu, [241]Am, [243]Am. The OSMOSE samples consist of a double zircaloy sheaths with the dimensions specified in Table 7 [15]:

Internal sheath [mm]	9.56
External sheath [mm]	10.6
Length [mm]	103.5

Table 8 - Dimensions of the OSMOSE samples

The matrix for all the samples is composed by natural uranium; for [237]Np and [241]Am two different sample have been chosen. The difference between two samples of the same nuclide is the mass of the minor actinide. The mass of all minor actinides are showed in Table 8 [15]:

Samples	Mass [g]
[237]Np/1	0.1
[237]Np/2	0.6
[242]Pu	0.5
[241]Am/1	0.06
[241]Am/2	0.2
[243]Am	0.5

Table 9 - Mass of the minor actinide in the samples

One of the samples is reported in Figure 65:
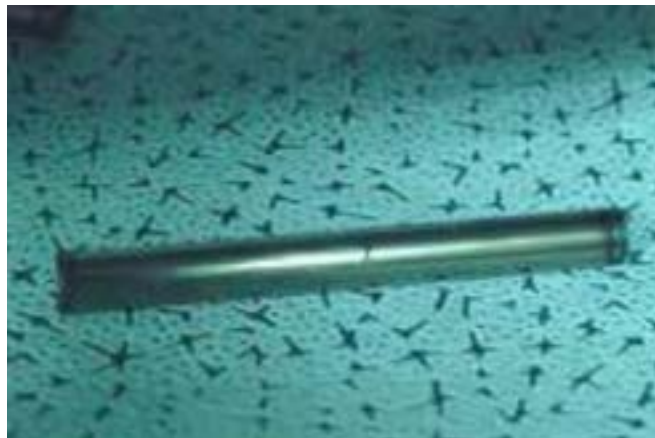
Figure 65 - OSMOSE sample.

The scheme followed to irradiate these samples, chosen as example, consists of a weekly scheme characterized by 5 hours of irradiation and 19 hours of cooling repeated for 4 times and after that 5 more hours of irradiation and 2 hours of cooling. Activity values are evaluated after these last 2 hours of cooling. The irradiation scheme is showed in Figure 66:
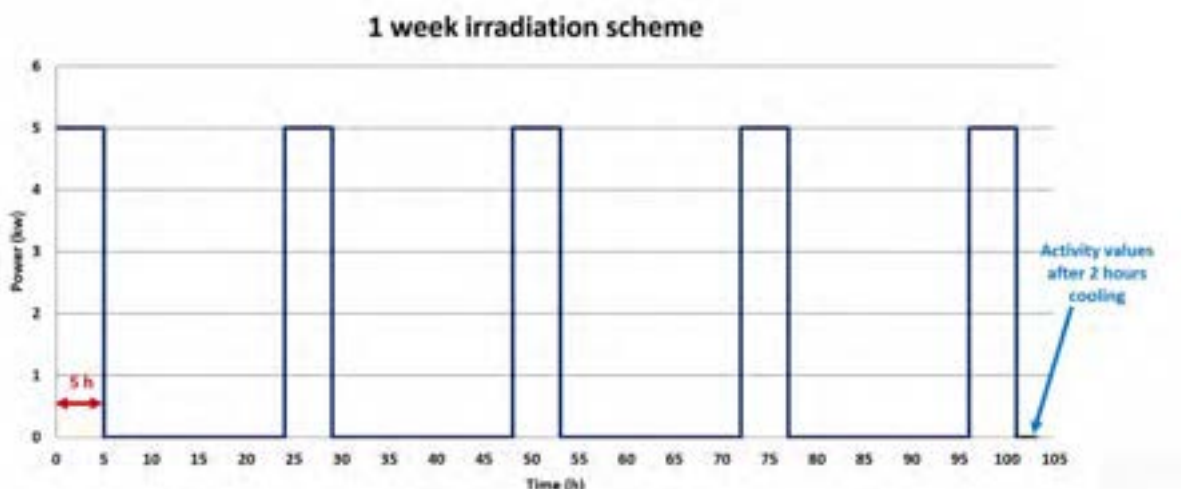
Figure 66 - One week irradiation scheme.

The (n, γ) capture reactions for the selected minor actinides are:

- $^{237}_{93}Np \rightarrow ^{238}_{93}Np$

- $^{242}_{94}Pu \rightarrow ^{243}_{94}Pu$

- $^{241}_{95}Am \rightarrow ^{242}_{95}Am$

- $^{243}_{95}Am \rightarrow ^{244}_{95}Am$

After the activation level determination of the samples, another important information that is necessary to consider is the development of the decay chains of the activated sample. Due to the different range of radioactive particles, the simplest radiation that can be measured through a detector is the γ and the X emission. For this reason it is important to know the energy of the γ (or X) ray emitted and their intensity (%). Obviously, for the same actinide this properties are constant. For each nuclide the only γ-ray considered is the most probable, the one with the biggest percentage intensity. In this way it is possible to define the best counting rates obtainable with the available detector. The activation chains taken into account are [16]:

- $^{237}_{93}Np \rightarrow ^{238}_{93}Np(2.117\ d)(\boldsymbol{\beta^-}) \rightarrow ^{238}_{94}Pu$

- $^{242}_{94}Pu \rightarrow ^{243}_{94}Pu(4.956\ h)(\boldsymbol{\beta^-}) \rightarrow ^{243}_{95}Am$

- $^{241}_{95}Am \rightarrow \begin{cases} ^{242}_{95}Am(16.02\ h)(\boldsymbol{\beta^-}: 82.7\%) \rightarrow ^{242}_{96}Cm \\ ^{242}_{95}Am(16.02\ h)(\boldsymbol{\varepsilon}: 17.3\%) \rightarrow ^{242}_{94}Pu \\ ^{242}_{95}Am(141\ y)(\boldsymbol{\alpha}) \rightarrow ^{238}_{93}Np \\ ^{242}_{95}Am(141\ y)(\boldsymbol{IT}: 99.55\%) \rightarrow ^{242}_{95}Am \end{cases}$

- $^{243}_{95}Am \rightarrow \begin{cases} ^{244}_{95}Am(26\ m)(\boldsymbol{\beta^-}:99.9639\%) \rightarrow\ ^{244}_{96}Cm \\ ^{244}_{95}Am(10.1\ h)(\boldsymbol{\beta^-}:100\%) \rightarrow\ ^{244}_{96}Cm \end{cases}$

While ^{238}Np and ^{243}Pu have one decay possibility, ^{242}Am have four different type of decay possibilities and ^{244}Am two. In this last two cases, the choice of the route depends on the parent half-life and on the detector efficiency that is characterized by a specific energy window.

After this considerations, for ^{242}Am the choice is between the first two routes[5] and in relation to the HPGe (High Purity Germanium) efficiency (described in the following pages) and to the intensity of the emitted γ, the better choice is represented by the second one. For ^{244}Am the chosen route is the second one because the intensity of the γ emission associated with the first route is negligible. The decay schemes of these nuclides are reported in Figure 67 and in Figure 68:
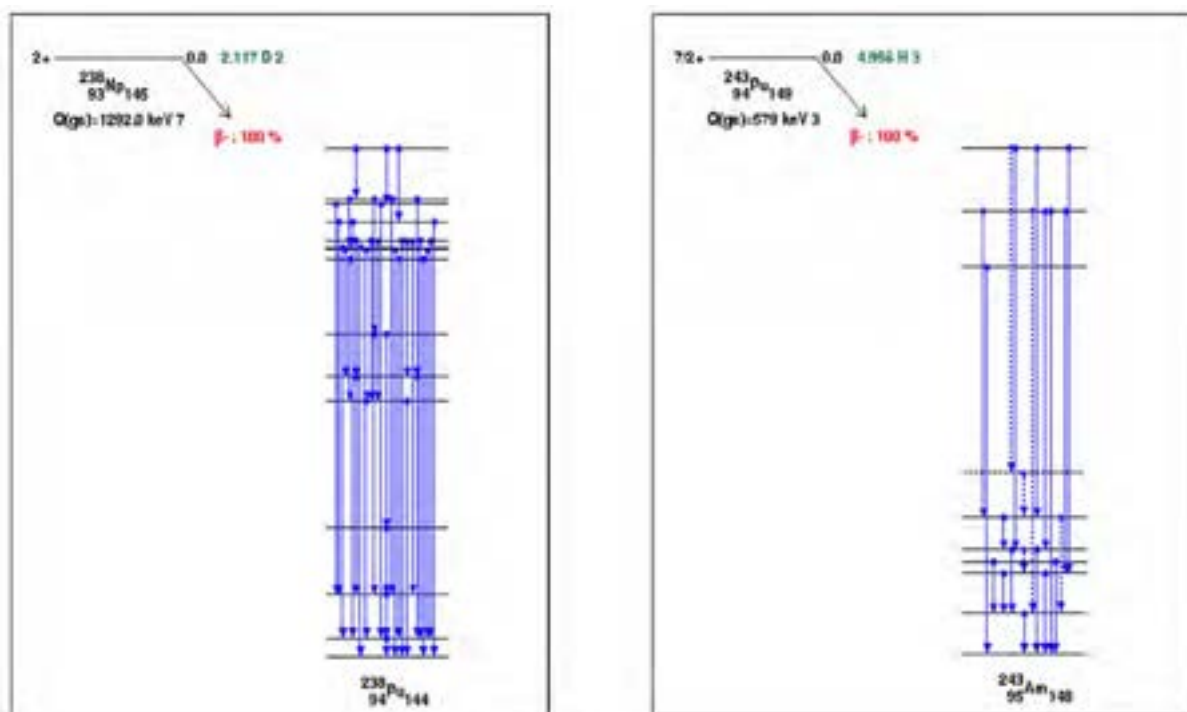
Figure 67 - Decay schemes for ^{238}Np and ^{243}Pu.

---

[5]Because of the too high half life of the last two.
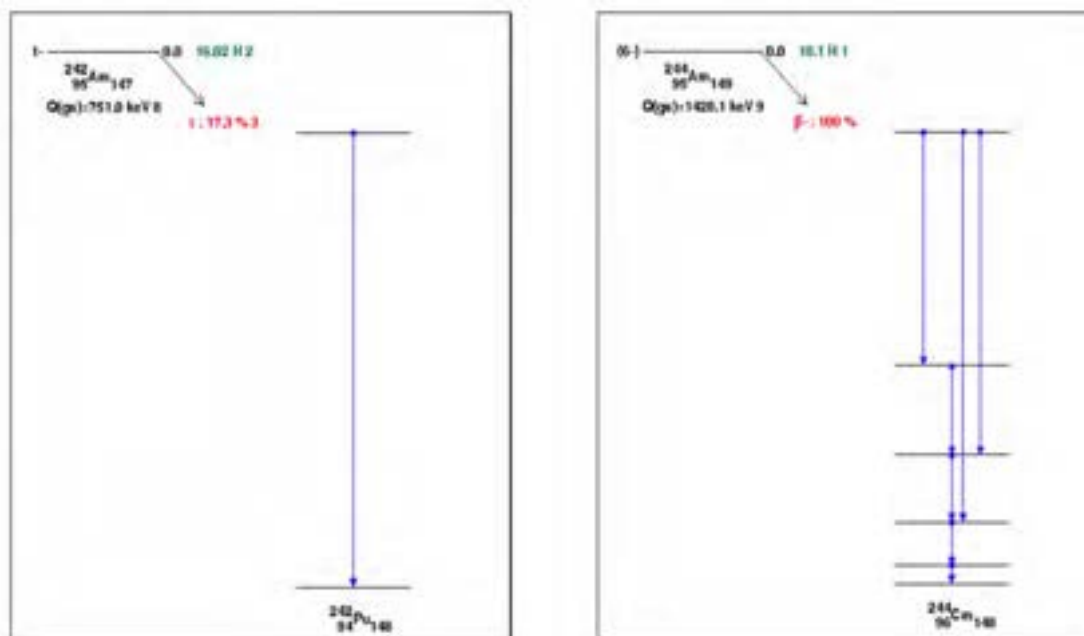
Figure 68 - Decay schemes for ^{242}Am and ^{244}Am.

Table 9 summarizes the energy and the intensity of the γ (or X) emission for each activation product [15].

	Position [cm]	r = 12.07	r = 24.58	r = 45.5
OSMOSE Samples	φ [n/cm^2 s]	7.44E+11	1.70E+11	5.97E+09
^{237}Np/1	^{238}Np γ-energy [keV]	984.45	984.45	984.45
	γ-intensity [%]	25.19	25.19	25.19
^{237}Np/2	^{238}Np γ-energy [keV]	984.45	984.45	984.45
	γ-intensity [%]	25.19	25.19	25.19
^{242}Pu	^{243}Pu γ-energy [keV]	84	84	84
	γ-intensity [%]	23.1	23.1	23.1
^{241}Am/1	^{242}Am $X_{k\alpha1}$-energy [keV]	103.374	103.374	103.374
	$X_{k\alpha1}$-intensity [%]	5.7	5.7	5.7
^{241}Am/2	^{242}Am $X_{k\alpha1}$-energy [keV]	103.374	103.374	103.374
	$X_{k\alpha1}$-intensity [%]	5.7	5.7	5.7
^{243}Am	^{244}Am γ-energy [keV]	743.971	743.971	743.971
	γ-intensity [%]	66	66	66

Table 10 - Activation products γ-energy and γ-intensity

These values, energy and intensity, are very important to evaluate the counting rate for each sample. The counting rate (cps or counts/s) can be evaluated using a very simple relations depending on the characteristics of the detector, in particular the detecting efficiency. The relation is:

$$C_r = A_i I_\gamma \varepsilon$$

where:
- ✓ A_i is the activity of the activation product [Bq];
- ✓ I_γ is the intensity of the γ or X emission [%];
- ✓ ε is the geometric efficiency of the detector [%].

The efficiency depend on the detector used for the evaluation. The detector is an ORTEC GMX series (Figure 69).

Thick contact (lithium diffusion)
500 - 1000 μm

Thin contact (ion implantation)
< 0.3 μm
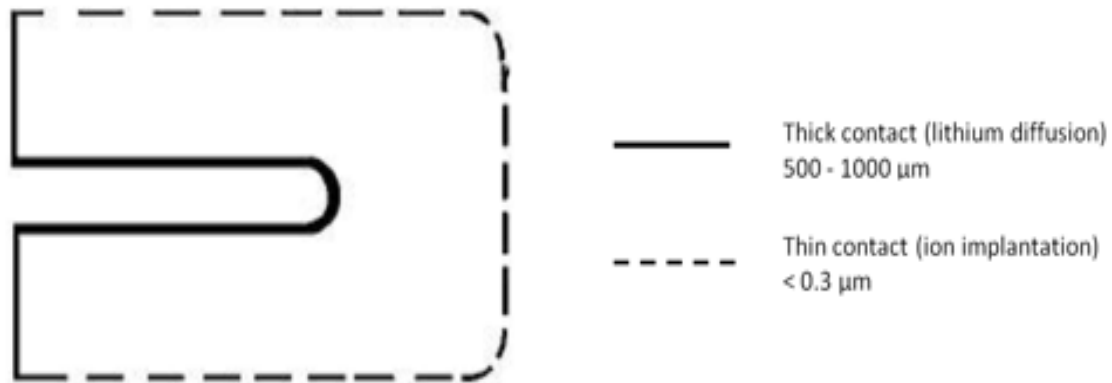
Figure 69 - HPGe detector

This is a n-type coaxial HPGe detector made of high purity germanium. It has a high precision and efficiency for both γ and x ray; the useful energy range is 3 keV÷10 MeV. In order to allow full benefit to this capabilities it is supplied with a large beryllium window. The characteristicdimensions are summarized in Table10

Crystal diameter [mm]	49.9
Crystal length [mm]	56.3
End cap to crystal [mm]	3
Beryllium layer [mm]	0.5
Inactive germanium [μm]	0.3

Table 11 - HPGe characteristic dimensions

The operating negative BIAS is around 3000 V, while the cool down time is 6 hours. About the detector efficiency, this can be expressed in the following Figure 70:

Figure 70 - Detector efficiency.

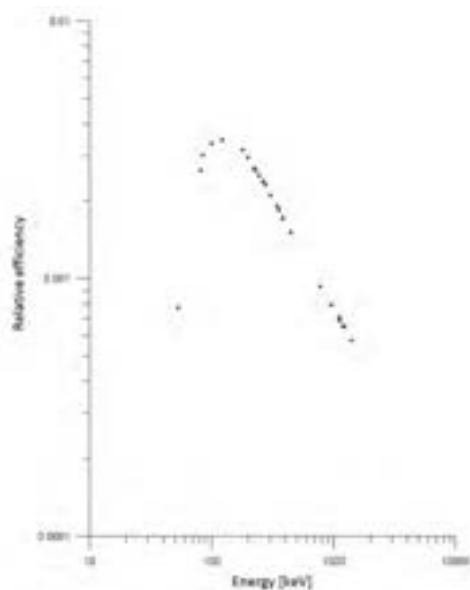Tables11-12 reports activity and capture cross sections values evaluated by FISPACT, in the three different position enounced previously and for fluxes evaluations by both codes.

	Position [cm]	r = 12.07	r = 24.58	r = 45.5
Osmose Samples	φ [n/cm^2 s]	7.44E+11	1.70E+11	5.97E+09
^{237}Np/1	σ_c [barn]	9.95E-01	1.74E+00	2.64E+01
	A_{Np-238} [Bq]	3.48E+07	1.39E+07	7.41E+06
	$A_{tot.}$ [Bq]	2.31E+10	3.59E+09	2.14E+09
^{237}Np/2	σ_c [barn]	9.95E-01	1.74E+00	2.64E+01
	A_{Np-238} [Bq]	2.09E+08	8.36E+07	4.44E+07
	$A_{tot.}$ [Bq]	2.49E+10	3.84E+09	2.19E+09
^{242}Pu	σ_c [barn]	3.22E-01	6.46E-01	3.21E+01
	A_{Pu-243} [Bq]	1.18E+08	5.38E+07	9.38E+07
	$A_{tot.}$ [Bq]	2.35E+10	3.67E+09	2.21E+09
^{241}Am/1	σ_c [barn]	1.27E+00	2.07E+00	4.59E+01
	A_{Am-242} [Bq]	3.56E+07	1.33E+07	1.04E+07
	$A_{tot.}$ [Bq]	3.04E+10	1.12E+10	9.73E+09
^{241}Am/2	σ_c [barn]	1.27E+00	2.07E+00	4.59E+01
	A_{Am-242} [Bq]	1.19E+08	4.44E+07	3.45E+07
	$A_{tot.}$ [Bq]	4.80E+10	2.89E+10	2.75E+10
^{243}Am	σ_c [barn]	1.09E+00	1.86E+00	4.69E+01
	A_{Am-244} [Bq]	2.17E+07	8.01E+06	6.78E+06
	$A_{tot.}$ [Bq]	2.94E+10	9.85E+09	8.41E+09

Table 12 - Activity values of OSMOSE samples by ERANOS fluxes.

Osmose Samples	Position [cm]	r = 12.07	r = 24.58	r = 45.5
	φ [n/cm^2 s]	6.87E+11	1.94E+11	1.46E+10
^{237}Np/1	σ_c [barn]	1.09E+00	2.29E+00	2.36E+01
	A_{Np-238} [Bq]	3.53E+07	2.09E+07	1.60E+07
	$A_{tot.}$ [Bq]	2.35E+10	5.78E+09	4.78E+09
^{237}Np/2	σ_c [barn]	1.09E+00	2.29E+00	2.36E+01
	A_{Np-238} [Bq]	2.12E+08	1.26E+08	9.60E+07
	$A_{tot.}$ [Bq]	2.52E+10	6.06E+09	4.87E+09
^{242}Pu	σ_c [barn]	3.84E-01	8.91E-01	2.61E+01
	A_{Pu-243} [Bq]	1.29E+08	8.47E+07	1.84E+08
	$A_{tot.}$ [Bq]	2.38E+10	5.79E+09	4.83E+09
^{241}Am/1	σ_c [barn]	1.25E+00	2.40E+00	3.62E+01
	A_{Am-242} [Bq]	3.52E+07	1.92E+07	2.14E+07
	$A_{tot.}$ [Bq]	3.08E+10	1.33E+10	1.24E+10
^{241}Am/2	σ_c [barn]	1.25E+00	2.40E+00	3.62E+01
	A_{Am-242} [Bq]	1.17E+08	6.39E+07	7.15E+07
	$A_{tot.}$ [Bq]	4.84E+10	3.10E+10	3.01E+10
^{243}Am	σ_c [barn]	8.16E-02	1.60E-01	2.57E+00
	A_{Am-244} [Bq]	2.17E+07	1.20E+07	1.44E+07
	$A_{tot.}$ [Bq]	2.97E+10	1.20E+10	1.10E+10

Table 13 - Activity values of OSMOSE samples by Serpent fluxes.

As showed, the values of the activity decrease moving towards the external part of the system, interested by a lower neutron flux, while the capture cross sections increase their values, according to the trends illustrated in the previous paragraphs. Obviously the results obtained differs due to the code used for the flux evaluation, but it can be seen that for all reactor positions and nuclides considered the results show the same trend.

Tables 13-14 collects the evaluated counting rate for the selected OSMOSE samples.

OSMOSE Samples	Position [cm]	r = 12.07	r = 24.58	r = 45.5
	φ [n/cm^2 s]	7.44E+11	1.70E+11	5.97E+09
^{237}Np/1	ε [%]	0.19	0.19	0.19
	C_r [cps]	16305	6531	3470
^{237}Np/2	ε [%]	0.19	0.19	0.19
	C_r [cps]	97830	39179	20822
^{242}Pu	ε [%]	0.53	0.53	0.53
	C_r [cps]	143978	65879	114864
^{241}Am/1	ε [%]	0.11	0.11	0.11
	C_r [cps]	2171	812	632
^{241}Am/2	ε [%]	0.11	0.11	0.11
	C_r [cps]	7233	2706	2106
^{243}Am	ε [%]	0.21	0.21	0.21
	C_r [cps]	30435	11262	9533

Table 14 - Counting rate for the selected samples for ERANOS fluxes.

	Position [cm]	r = 12.07	r = 24.58	r = 45.5
OSMOSE Samples	φ [n/cm^2 s]	6.87E+11	1.94E+11	1.46E+10
^{237}Np/1	ε [%]	0.19	0.19	0.19
	C_r [cps]	16900	10013	7658
^{237}Np/2	ε [%]	0.19	0.19	0.19
	C_r [cps]	101417	60066	45937
^{242}Pu	ε [%]	0.53	0.53	0.53
	C_r [cps]	158424	103735	225761
^{241}Am/1	ε [%]	0.11	0.11	0.11
	C_r [cps]	2208	1202	1344
^{241}Am/2	ε [%]	0.11	0.11	0.11
	C_r [cps]	7361	4006	4481
^{243}Am	ε [%]	0.21	0.21	0.21
	C_r [cps]	30104	16660	19903

Table 15 - Counting rate for the selected samples for Serpent fluxes.

It is evident that the obtained results shows high level for the counting rate; however, these results are even too high because of the activity level reached by the samples. These values need to be reduced according to the total admissible activity for radiological issue.

These results allow to predict the feasibility of such type of measurements and detailed analysis will be carry out in the next future with the principal aim to realize an experimental campaign.

12. Conclusions

The aim of this work is to evaluate the feasibility to perform an irradiation of minor actinides samples in the TAPIRO fast reactor. The preliminary neutronic evaluation of TAPIRO reactor is carried out with the French deterministic code ERANOS, the Monte Carlo code SERPENT and MCNP. The analysis of the flux and the neutron spectrum in different positions along the diametrical channel have been analyzed. The feasibility of the results was verified by a comparison between three different code evaluations: ERANOS, SERPENT and MCNP.

Thanks to the flux calculation, it was possible to obtain some information about the system, such as the reaction rates, the average microscopic cross section and the capture-to-fission ratio of selected minor actinides.

The second part of the work is focused on the activation calculations, performed with FISPACT calculation code.

According to CEA, a list of OSMOSE samples of minor actinides was chosen. Using FISPACT code it is possible to evaluate the activity of these samples after a cycle of irradiation inside the reactor, in different reactor positions among diametrical channel. Considering the values of activity, and the energy of the γ emitted by the samples, the counting rate of each samples, obtained using a HPGe, has been determined.

The encouraging results show high level for the counting rate and allows to predict the feasibility of such type of measurements. A detailed analysis will be carry out in the next future to realize an experimental campaign, named AOSTA (Activation of OSMOSE Samples in TAPIRO), in an ENEA - CEA collaboration.

13. References.

1. http://www.enea.it/en/research-development/documents/nuclear-fission/tapiro-eng-pdf

2. N. Burgio, A. Santagata, M.Frullini, F. La Stella, F. Garofalo, C. Rusconi, "Reinterpretation of the late SCK-CEN/ENEA Experimental Neutronic Campaign on TAPIRO Fast Reactor with MCNPX Monte Carlo Transport Code", ENEA, Report RdS/2012/042, September 2012

3. G. Rimpault et al., "The ERANOS code and data system for fast reactor neutronic analyses", Proc. PHYSOR 2002, Seoul, Korea, October 7-10, 2002.

4. G. Rimpault, "Physics documentation of the ERANOS. The ECCO cell code", CEA Technical Note RT-SPRC-LEPh-97-001, 1997.

5. G. Palmiotti, "BISTRO: BIdimensionnel Sn Transport Optimise", CEA Technical NOTE NT-SPRC-LEPh-84-270, 1984.

6. http://montecarlo.vtt.fi/

7. J. Leppanen, Development of a New Monte Carlo Reactor Physics Code, VTT publications, 2007.

8. J.T. Goorley, et al., "Initial MCNP6 Release Overview - MCNP6 version 1.0", LA-UR-13-22934 (2013)

9. http://www.ccfe.ac.uk/EASY.aspx

10. R. A. Forrest, "FISPACT-2007: User manual", EASY Documentation Series, EURATOM/UKAEA Fusion Association, Culham Science Centre.

11. J. -Ch. Sublet, L. W. Parker, J. Kopecky, R. A. Forrest, A. J. Koning, D. A. Rochman, "The European Activation File: EAF-2010 neutron-induced cross section library", EASY Documentation Series.

12. M. Carta, M. Palomba, "TRIGA RC-1 and TAPIRO, ENEA Research Reactors", ENEA, Italian National Agency for New Technologies, Energy and Sustainable Economic Development C.R Casaccia, Wien, June 10-12, 2013.

13. G. Youinou, G. Palmiotti, M. Salvatores, G. Imel, R. Pardo, F. Kondev, M. Paul, "Principle and Uncertainty Quantification of an Experiment Designed to Infer Actinide Neutron Capture Cross-Sections", INL, January 2010.

14. P.Weiss, Neptunium Nukes? Little-studied metal goes critical, Science Newes, 26/10/2013.

15. F. Boccia, M. Carta, V. Fabrizio, A. Grossi, C. Bethaz, B. Geslot, P. Blaise, A. Gruel, "Analysis of OSMOSE samples in TAPIRO for MA capture cross sections measurements", CEA - ENEA, OECD/NEA NSC EGIEMAM-II meeting, Paris, April 29 - 30, 2015.

16. Interactive chart of nuclides: http://www.nndc.bnl.gov/chart